Geochemistry Geophysics Geosystems G3

Article
Volume 12, Number 9
17 September 2011
Q09009, doi:10.1029/2011GC003575
ISSN: 1525-2027

Published by AGU and the Geochemical Society

Distribution and abundance of gas hydrates in near-surface deposits of the Håkon Mosby Mud Volcano, SW Barents Sea

Thomas Pape
MARUM–Center for Marine Environmental Sciences and Department of Geosciences, University of Bremen, Klagenfurter Strasse, D-28334 Bremen, Germany (tpape@marum.de)

Tomas Feseker
MARUM–Center for Marine Environmental Sciences and Department of Geosciences, University of Bremen, Klagenfurter Strasse, D-28334 Bremen, Germany

Leibniz Institute of Marine Sciences at University of Kiel (IFM-GEOMAR), Wischhofstrasse 1-3, D-24148 Kiel, Germany

Sabine Kasten
Alfred Wegener Institute for Polar and Marine Research, Am Handelshafen 12, D-27570 Bremerhaven, Germany

David Fischer
MARUM–Center for Marine Environmental Sciences and Department of Geosciences, University of Bremen, Klagenfurter Strasse, D-28334 Bremen, Germany

Alfred Wegener Institute for Polar and Marine Research, Am Handelshafen 12, D-27570 Bremerhaven, Germany

Gerhard Bohrmann
MARUM–Center for Marine Environmental Sciences and Department of Geosciences, University of Bremen, Klagenfurter Strasse, D-28334 Bremen, Germany

[1] The occurrence of gas hydrates at submarine mud volcanoes (MVs) located within the gas hydrate stability zone (GHSZ) is controlled by upward fluid and heat flux associated with MV activity. Determining the spatial distribution of gas hydrates at MVs is crucial to evaluate their sensitivity to known episodic changes in volcanic activity. We determined the hydrocarbon inventory and spatial distribution of hydrates at an individual MV structure. The Håkon Mosby Mud Volcano (HMMV), located at 1,250 m water depth on the Barents Sea slope, was investigated by combined pressure core sampling, heat flow measurements, and pore water chemical analysis. Quantitative pressure core degassing revealed gas–sediment ratios between 3.1 and 25.7, corresponding to hydrate concentrations of up to 21.3% of the pore volume. Hydrocarbon compositions and physicochemical conditions imply that gas hydrates incipiently crystallize as structure I hydrate, with a dissociation temperature of around 13.8°C at this water depth. Based on numerous in situ measurements of the geothermal gradient in the seabed, pore water sulfate profiles and microbathymetric data, we show that the thickness of the GHSZ increases from less than 1 m at the warm center to around 47 m in the outer parts of the HMMV. We estimate the total mass of hydrate-bound methane stored at the HMMV to be about 102.5 kt, of which 2.8 kt are located within the morphological Unit I around the center and thus are likely to be dissociated in the course of a large eruption.

Copyright 2011 by the American Geophysical Union

Components: 13,000 words, 11 figures, 6 tables.

Keywords: Dynamic Autoclave Piston Corer; Håkon Mosby Mud Volcano; gas hydrates; in situ temperature; methane; pore water sulfate.

Index Terms: 3004 Marine Geology and Geophysics: Gas and hydrate systems; 3015 Marine Geology and Geophysics: Heat flow (benthic); 8426 Volcanology: Mud volcanism (4302).

Received 21 February 2011; **Revised** 14 July 2011; **Accepted** 17 July 2011; **Published** 17 September 2011.

Pape, T., T. Feseker, S. Kasten, D. Fischer, and G. Bohrmann (2011), Distribution and abundance of gas hydrates in near-surface deposits of the Håkon Mosby Mud Volcano, SW Barents Sea, *Geochem. Geophys. Geosyst.*, *12*, Q09009, doi:10.1029/2011GC003575.

1. Introduction

[2] Fluids ascending at submarine mud volcanoes (MVs) supply significant amounts of heat, fluidized mud and light hydrocarbons such as methane into shallow deposits and the water column [*Dimitrov*, 2002; *Etiope and Klusman*, 2002; *Kopf*, 2002; *Kvenvolden and Rogers*, 2005]. The fate of hydrocarbons accumulated in and released from submarine MVs is of great interest, since they promote significant biogeochemical processes in near-surface sediments and in the water column, and can act as greenhouse gases in the atmosphere [*Etiope and Klusman*, 2002; *Etiope and Ciccioli*, 2009; *Milkov et al.*, 2003b].

[3] Within gas-laden deep-sea sediments, such as shallow deposits of submarine MVs, volatile hydrocarbons separate into different phases. These include free gas, gas dissolved in interstitial waters, and when located within the gas hydrate stability zone (GHSZ), hydrate-bound gas. MV associated gas hydrates were reported from several oceans worldwide [*Bohrmann et al.*, 2003; *Chazallon et al.*, 2007; *Ivanov et al.*, 1996; *Limonov et al.*, 1994; *Milkov*, 2000; *Pape et al.*, 2010b; *Vogt et al.*, 1997; *Woodside et al.*, 1998]. Submarine gas hydrates are of great interest since they are a globally relevant reservoir of methane and higher hydrocarbon [*Bohrmann and Torres*, 2006; *Kvenvolden*, 1988; *Pape et al.*, 2010b; *Sloan and Koh*, 2007]. However, gas hydrates are highly sensitive to changes in heat flux and respond rapidly to such variations by decomposition and gas release when sediment temperatures reach hydrate dissociation temperatures, for instance during active mud volcanic phases. Our previous study on the Dvurechenskii MV in the Northeastern Black Sea revealed that variations in heat flow were compensated by hydrate dissociation and formation rather than leading to changes in sediment temperature [*Feseker et al.*, 2009b].

[4] Plumes of light hydrocarbons as well as extensive gas bubble streams indicative for active gas discharge into the water column were reported from MVs in several ocean areas, such as the Eastern Mediterranean [*Charlou et al.*, 2003], the Black Sea [*Greinert et al.*, 2006; *Sahling et al.*, 2009], the Barents Sea [*Sauter et al.*, 2006], and the Gulf of Cadiz [*Mazurenko et al.*, 2003]. Estimates of the global number of submarine MVs range between 10^3 and 10^5 [*Dimitrov*, 2002; *Milkov*, 2000]. The total amount of hydrocarbons stored in MV deposits and the global gas flux from MVs into the water column and potentially into the atmosphere is still openly debated [*Dimitrov*, 2002, 2003; *Etiope et al.*, 2008; *Kopf*, 2002, 2003; *Kvenvolden and Rogers*, 2005; *Milkov et al.*, 2003b; *Milkov*, 2004; *Milkov and Etiope*, 2005]. This is mainly due to insufficient seafloor coverage by high resolution mapping methods and to the technical effort required to determine in situ gas and gas hydrate concentrations (i.e., pressure sampling techniques) in deep sea sediments. Moreover, episodic activity observed at most MVs [e.g., *Deville and Guerlais*, 2009; *Feseker et al.*, 2009a; *Greinert et al.*, 2006; *Kopf*, 2002; *Vanneste et al.*, 2011], complicates the estimation of gas emissions from individual MVs. Nonetheless, ex situ concentrations of light hydrocarbons in shallow deposits and annual methane emissions were reported for selected structures [e.g., *Blinova et al.*, 2003; *Felden et al.*, 2010; *Mastalerz et al.*, 2007; *Niemann et al.*, 2006a; *Sahling et al.*, 2009; *Sauter et al.*, 2006; *Stadnitskaia et al.*, 2006].

[5] The spatial distribution of hydrates in MV deposits is controlled by the flux of warm and sulfate-free fluids from below, which determines sediment temperature, methane concentration, and thickness of the zone of microbial methane consumption. Figure 1 shows a general scheme of the hydrate distribution in shallow MV deposits. Hydrates form where methane concentrations exceed

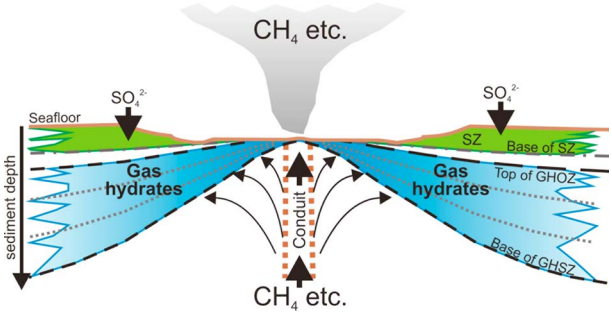

Figure 1. Cross section illustrating typical gas hydrate (GH) distributions in shallow deposits of submarine mud volcanoes (modified after *Bohrmann and Torres* [2006]) indicating temperature isolines, the base of the gas hydrate stability zone (BGHSZ), and the top of the gas hydrate occurrence zone (GHOZ). Hydrocarbons including methane along with heat ascend through a central conduit toward the seafloor. Within the sulfate zone (SZ), methane is microbially consumed, which affects the relative position of the top of the GHOZ.

aqueous solubility and sediment temperatures are below the hydrate dissociation temperature, i.e., above the base of the gas hydrate stability zone (BGHSZ). During mud volcanic eruptions, the upward flux of warm fluids through one or more conduits toward the seafloor leads to a temporal (and spatially restricted) temperature increase, which may cause a local upward shift of the BGHSZ, destabilization of hydrates, and increased methane release from the seabed into the bottom water. In this study we concentrate on the depth interval where gas hydrates actually occur. This site-specific gas hydrate occurrence zone (GHOZ) is located below the sulfate zone (SZ) and has to be distinguished from the GHSZ, where pressure and temperature provide hydrate stability, but gas hydrate may not be present due to the lack of sufficient methane concentrations [e.g., *Milkov*, 2004; *Paull et al.*, 2005].

[6] At shallow sediment depth, aerobic and anaerobic oxidation of methane may keep methane concentrations below saturation and thus prevent gas hydrate formation. In addition, the fluid flow decreases with increasing distance to the conduit and allows seawater-derived sulfate to penetrate into the sediments and to promote the sulfate-dependent anaerobic oxidation of methane (AOM) [*Barnes and Goldberg*, 1976; *Hoehler et al.*, 1994; *Reeburgh*, 1976]. The respective methane depletion results in a deepening of the top of the GHOZ as a function of increasing distance from the conduit (Figure 1). Due to upward methane diffusion, a cm to dm thick interval characterized by the absence of sulfate and low methane concentrations should occur between the base of the SZ and the top of the GHOZ [*Paull et al.*, 2005]. Nonetheless, in the absence of more accurate means of measurement, the base of the SZ may be taken as an upper limit of the GHOZ.

[7] To the best of our knowledge only one study on in situ hydrocarbon concentrations in shallow deposits of individual MVs exists [*Pape et al.*, 2010b]. In the present study, we determined in situ temperature gradients as well as concentrations of methane, sulfate and chloride in order to estimate the amount and spatial distribution of gas hydrates in near-surface deposits of the Håkon Mosby MV located in the Southwestern Barents Sea. Our results provide new quantitative information to the still sparse global data set on in situ gas and hydrate amounts present in deposits of deep-sea MVs.

2. Study Area and Methods

2.1. Study Area

[8] The Håkon Mosby Mud Volcano (HMMV) is located on the margin between the Southwestern Barents Sea and the Norwegian Sea (Figure 2) at about 1,250 to 1,270 m water depth [*Foucher et al.*, 2009; *Hjelstuen et al.*, 1999; *Vogt et al.*, 1997]. It is about 1.4 km in diameter and covers a seafloor area of ca. 1.395 km^2 [*Jerosch et al.*, 2007]. Seismic investigations revealed mud volcanic activity since about 330 ka before present and a pseudomud chamber positioned at a depth of about 300 m below seafloor (bsf) which fuels focused and rapid fluid flow through a comparably narrow vertical conduit [*Perez-Garcia et al.*, 2009]. Expelled fluids evidently originated from preglacial deposits that became pressurized by sediment loading from ~3 km thick glacial sequences [*Hjelstuen et al.*, 1999; *Perez-Garcia et al.*, 2009]. A rapid extrusion of relatively low viscosity mud comprised of silty to sandy mud and bearing clasts (mud breccia) is suggested by a flat morphology with maximum bathymetric relief of about 16 m [*Foucher et al.*, 2010; *Jerosch et al.*, 2007; *Milkov et al.*, 1999, 2004b; *Perez-Garcia et al.*, 2009].

[9] Episodic peaks in mud volcanic activity at the HMMV are indicated by a high temporal variability in sediment temperatures observed between 2003 and 2007 [*Feseker et al.*, 2008; *Kaul et al.*, 2006] which is assumed to generate a highly dynamic hydrate system. Recent mud volcanic activity was

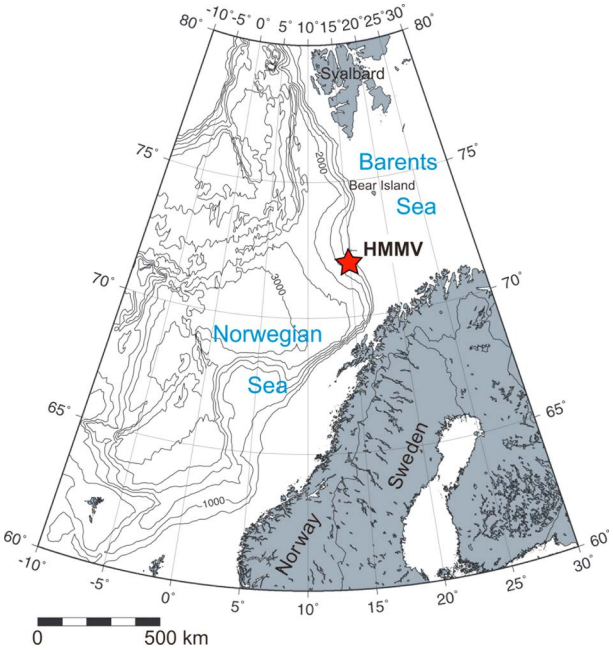

Figure 2. The Håkon Mosby Mud Volcano (HMMV) located on the Barents Sea slope between Norway and Svalbard. The contour interval is 500 m.

substantiated by subtle morphological changes over the entire crater over a period of 3 years [*Foucher et al.*, 2010], methane concentration anomalies in sediments and bottom waters above the central zone [*Damm and Budeus*, 2003], gas bubble emission from the seafloor north of the geometric center [*Charlou et al.*, 2007; *Foucher et al.*, 2010; *Sauter et al.*, 2006], as well as the widespread occurrence of gas hydrates in shallow sediments [*Egorov et al.*, 1999; *Ginsburg et al.*, 1999; *Jerosch et al.*, 2007; *Milkov et al.*, 2004b; *Vogt et al.*, 1997]. Considering an annual advective flux of methane of 18.9 * 10^6 mol yr^{-1} determined for three vent sites [*Sauter et al.*, 2006], the HMMV is suggested to represent a significant source of methane into the water column [cf. *Sahling et al.*, 2009]. In addition, estimated annual diffusive methane effluxes from the total HMMV structure (13.5 * 10^6 mol yr^{-1} [*Felden et al.*, 2010]) were in the same range as gaseous methane fluxes.

[10] During ROV inspections performed during R/V *Polarstern* cruise ARK-XXII/1b in 2007, bubble emission from the HMMV could not be observed, although acoustic flares indicating gas bubble ascent in the water column were recognized (unpublished data). Nevertheless, mud volcanic activity provoking changes in the morphology [*Foucher et al.*, 2010] and sediment thermal structures [*Feseker et al.*, 2008; *Kaul et al.*, 2006], bubble escape into bottom waters [*Foucher et al.*, 2010; *Sauter et al.*, 2006], and methane anomalies in the water column [*Damm and Budeus*, 2003; *Sauter et al.*, 2006] observed during several cruises in previous years provides strong evidence for a highly dynamic gas and gas hydrate inventory at the HMMV.

[11] The steep geochemical gradients induced by the upward migration of fluids and heat promote the settlement of the sediment surface by distinct microbial communities [*de Beer et al.*, 2006; *Lein et al.*, 1999; *Lösekann et al.*, 2007; *Milkov et al.*, 2004b; *Niemann et al.*, 2006b]. For instance, methane concentrations sustaining hydrate formation at the HMMV are strongly affected by both, aerobic methanotrophy [*Hanson and Hanson*, 1996] in the center and the sulfate-dependent anaerobic oxidation of methane (AOM [*Barnes and Goldberg*, 1976; *Hoehler et al.*, 1994; *Reeburgh*, 1976]) in peripheral areas. At the HMMV, AOM occurred in near-surface sediments distant to the center where seawater-derived sulfate could penetrate [*de Beer et al.*, 2006; *Felden et al.*, 2010; *Lichtschlag et al.*, 2010; *Lösekann et al.*, 2007; *Niemann et al.*, 2006b]. In contrast, aerobic methanotrophy, which is restricted to the upper few decimeters of the seafloor, as this process only occurs in (micro)aerated habitats, was found in shallow deposits at the center [*Elvert and Niemann*, 2008; *Lösekann et al.*, 2007; *Niemann et al.*, 2006b]. Combined with topographic features, these observations led to the classification of morphological units and biological zones, respectively [*Felden et al.*, 2010; *Jerosch et al.*, 2007; *Lichtschlag et al.*, 2010; *Niemann et al.*, 2006b]. With respect to the objectives of this study we herein follow the classification proposed by *Jerosch et al.* [2007]. Briefly, the so-called Unit I comprises both, a flat central area populated by aerobic methanotrophs and an adjacent zone largely colonized by *Beggiatoa* mats [*Felden et al.*, 2010; *Lichtschlag et al.*, 2010; *Lösekann et al.*, 2007; *Niemann et al.*, 2006b]. The central area is characterized by steepest temperature gradients and highest temperatures, and is the predominant zone of diffusive methane efflux from the HMMV [*Felden et al.*, 2010; *Feseker et al.*, 2008; *Foucher et al.*, 2010; *Kaul et al.*, 2006]. Unit I is surrounded by a transition zone, which is marked by patches of microbial mats, and a widespread hummocky outer zone densely inhabited by siboglinid tubeworms. Both zones belong to the Unit II. The outermost morphological Unit of the HMMV, Unit III, is represented by a pronounced

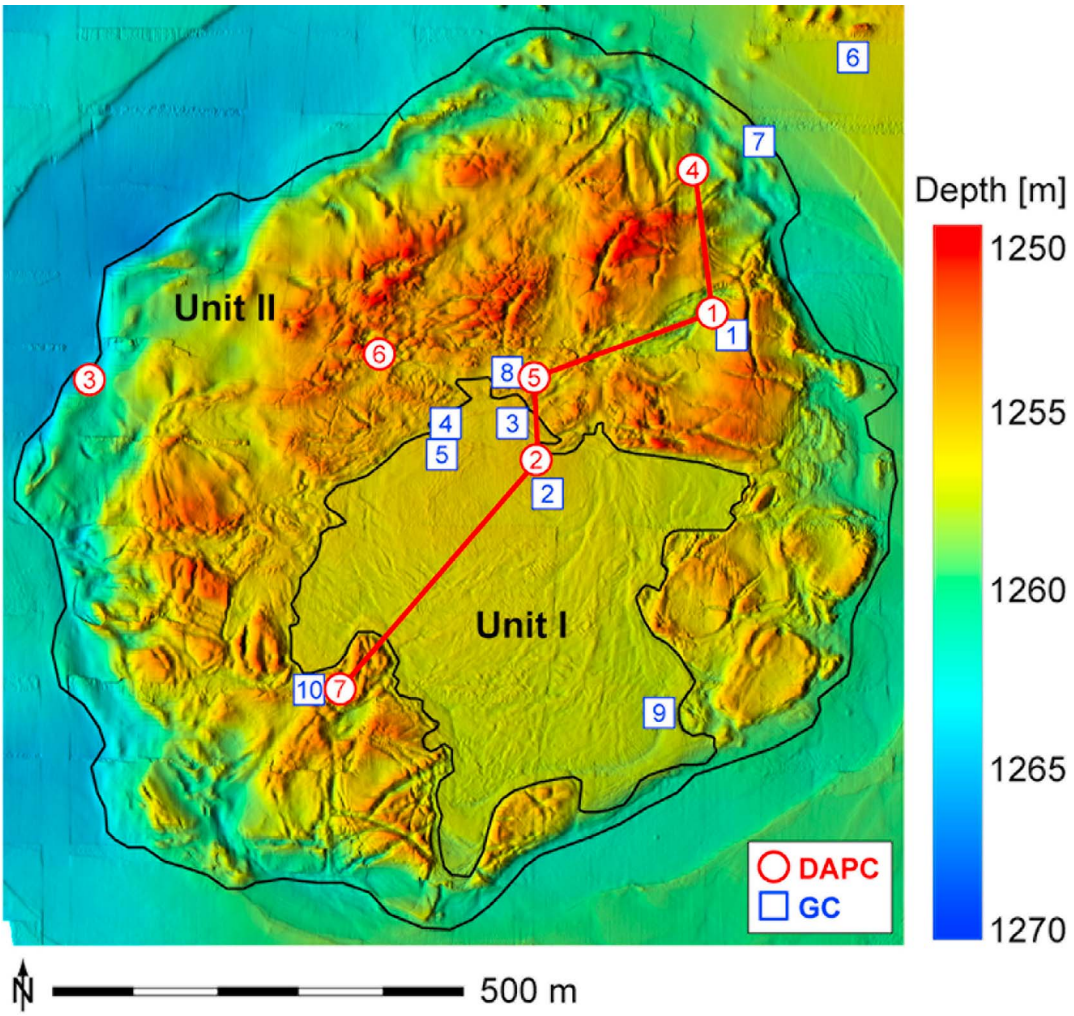

Figure 3. Limits of morphological Units I and II of the HMMV area (black lines [after *Jerosch et al.*, 2007]) and sampling stations during cruise PS 70 ARK-XXII/1b. DAPC (Dynamic Autoclave Piston Corer) and GC (Gravity Corer) stations are indicated in red circles and blue squares, respectively. The red line shows the SW-NE trending transect along which sulfate penetration, temperature gradient, and hydrate thickness are illustrated in Figure 11 (microbathymetry data from *Foucher et al.* [2009]).

moat surrounding the entire MV [*Jerosch et al.*, 2007].

[12] Very high in situ temperatures of more than 20°C in shallow sediments in the central area of the HMMV with respect to bottom water temperatures of around –0.8°C correspond to extremely high temperature gradients exceeding 40°C m^{-1} [*Feseker et al.*, 2008; *Foucher et al.*, 2010; *Kaul et al.*, 2006]. The high heat flux at the center strongly impacts the boundaries of the GHOZ in HMMV near-surface sediments and is assumed to result in a watch glass-shaped hydrate distribution profile in a cross section of the central conduit and surrounding field (Figure 1). Maximum hydrate concentrations approaching 25% of the bulk sediment volume and an average concentration of 1.2% for the entire HMMV were inferred from pore water chloride profiles in a previous study [*Ginsburg et al.*, 1999]. Accordingly, the amount of hydrate-bound gas in HMMV deposits was estimated at 3 * 10^8 m^3 (at Standard Temperature and Pressure, STP) [*Ginsburg et al.*, 1999]. With regard to gas compositions published for hydrates and sediments collected from the HMMV, the amount of hydrate-bound gas corresponds to 1.3 * 10^{10} mol methane, which is approx. 400 times the total methane mass annually released by gaseous and diffusive efflux [*Felden et al.*, 2010; *Milkov et al.*, 2004b; *Sauter et al.*, 2006]. However, no attempts have been made to investigate the exact distribution of hydrates in

Table 1. Station Characteristics of Nonpressurized (GC) and Pressurized (DAPC) Sediment Cores Recovered From the Håkon Mosby Mud Volcano During ARK-XXII/1b in Summer 2007

Station	Running Number	Latitude (°N)	Longitude (°E)	Morphological Unit	Remarks
		Gravity Cores (GC)			
54-1	1	72:0.368[a]	14:44.070[a]	II	gas hydrates
69-1	2	72:0.265	14:43.686	I	
92-1[a]	3	72:0.31[a]	14:43.61[a]	I	gas hydrates
93-1[a]	4	72:0.31[a]	14:43.47[a]	I	gas hydrates
94-1[a]	5	72:0.29[a]	14:43.46[a]	I	gas hydrates
98-1	6	72:0.550	14:44.325	III	
102-1	7	72:0.495	14:44.127	II	gas hydrates
110-1	8	72:0.344	14:43.622	II	gas hydrates
117-1	9	72:0.122	14:43.920	I	
122-1	10	72:0.135	14:43.236	II	gas hydrates
		Pressurized Cores (DAPC)			
53-1	1	72:0.383[a]	14:44.035[a]	II	
68-1	2	72:0.287[a]	14:43.667[a]	I	
81-1	3	72:0.338	14:42.724	II	
97-1	4	72:0.476	14:43.994	II	
113-1	5	72:0.340	14:43.659	II	
126-1	6	72:0.355	14:43.333	II	
133-1	7	72:0.137	14:43.255	II	

[a]Ship position.

shallow sediments of the HMMV and their sensitivity to changes in the sediment temperature regime.

2.2. Methods

2.2.1. Seafloor Sampling, Gas Quantification, and Gas and Pore Water Analysis

[13] For groundtruthing, both nonpressurized and pressurized sediment cores were recovered with a gravity corer (GC) and the Dynamic Autoclave Piston Corer (DAPC) [*Abegg et al.*, 2008; *Heeschen et al.*, 2007; *Pape et al.*, 2010a], respectively (Figure 3 and Table 1). High precision underwater navigation and positioning was achieved for most GC and DAPC stations by deploying an acoustic transponder (POSIDONIA, IXSEA) mounted on the wire 50 m above the sampling devices. Nonpressure cores were recovered from sites located in Units I to III according to the classification proposed by *Jerosch et al.* [2007], whereas pressure core stations were exclusively retrieved from Units I and II (Figure 3).

[14] For the inspection of shallow gas hydrate occurrences at specific sites and retrieval of intact hydrate pieces, a conventional GC equipped with a 5 m core barrel was used at ten stations. For long-term storage and molecular analyses of hydrate-bound gas onshore, near-surface gas hydrates were placed into gas-tight syringes to decompose under atmospheric conditions. The gas released was transferred into sealed glass vials prefilled with concentrated sodium chloride solution [*Pape et al.*, 2010a].

Table 2. General Characteristics of Pressure Cores Taken During ARK-XXII/1b at the HMMV

DAPC	Morphological Unit	Core Recovery (cm)	Recovery Pressure (bar)	Core Volume V_c (mL)	Gas Volumes Released V_{tg} (mL)	Gas Volume/Core Volume (mL mL^{-1})
1	II	254.5	105.9	13,598	231,200 ± 6,936	17.0 ± 0.5
2	I	240.0	87.9	12,823	65,100 ± 1,953	5.1 ± 0.2
3	II	265.0	107.7	14,159	37,200 ± 1,116	2.6 ± 0.1
4	II	270.0	104.1	14,426	200,500 ± 6,015	13.9 ± 0.4
5	II	260.0	129.9	13,892	200,350 ± 6,010	14.4 ± 0.4
6	II	n.d.[a]	128.9	2,650	189,000 ± 5,670	71. 3[b]
7	II	170.0	n.d.[a]	9,083	228,900 ± 6,867	25.2 ± 0.8

[a]Not determined.
[b]Estimate.

Table 3. Distribution of C_1 Through n-C_4 Hydrocarbons (as mol % of $\Sigma[C_1 - n\text{-}C_4]$) in Gas Released From Decomposing Gas Hydrates and During Controlled Degassing of Pressure Cores

Running Number	Morphological Unit	C_1	C_2	C_3	i-C_4	n-C_4	C_1/C_{2+}	C_1/C_2	C_1/C_3
				Pressure Cores (DAPC)					
2	I	99.9018	0.0907	0.0049	0.0020	0.0005	1,018	1,101	20,251
1	II	99.9126	0.0853	0.0018	0.0002	tr.[a]	1,144	1,172	54,181
3	II	99.9352	0.0637	0.0010	tr.[a]	tr.[a]	1,542	1,568	97,262
4	II	99.9063	0.0914	0.0020	0.0003	tr.[a]	1,066	1,093	50,385
5	II	99.9348	0.0608	0.0034	0.0009	0.0001	1,533	1,643	29,159
6	II	99.9088	0.0872	0.0030	0.0010	0.0001	1,095	1,146	33,066
7	II	99.9164	0.0814	0.0018	0.0004	tr.[a]	1,195	1,227	56,289
Mean DAPC, Unit II		99.9190	0.0783	0.0022	0.0005	tr.[a]	1,234	1,276	45,841
				Gas Hydrates (GC)					
3	I	99.9118	0.0784	0.0066	0.0029	0.0002	1,133	1,274	15,115
4	I	99.9420	0.0523	0.0043	0.0013	tr.[a]	1,724	1,909	23,298
5	I	99.9177	0.0799	0.0021	0.0003	tr.[a]	1,215	1,250	48,379
Mean GC, Unit I		99.9239	0.0702	0.0043	0.0015	0.0001	1,357	1,478	28,931
1	II	99.9134	0.0847	0.0017	0.0002	tr.[a]	1,153	1,180	57,460
7	II	99.9440	0.0238	0.0220	0.0097	0.0005	1,786	4,199	4,548
8	II	99.9389	0.0585	0.0021	0.0005	tr.[a]	1,637	1,708	48,018
10	II	99.9417	0.0561	0.0018	0.0004	tr.[a]	1,716	1,782	55,252
Mean GC, Unit II		99.9345	0.0558	0.0069	0.0027	0.0001	1,526	1,792	14,482

[a]Trace (tr.) = <0.0001 mol %.

[15] Seven pressurized near-surface sediment cores (Figure 3 and Tables 1 and 2) of a total maximum length of 2.65 m were recovered during expedition ARK-XXII/1b using the DAPC [*Abegg et al.*, 2008; *Heeschen et al.*, 2007; *Pape et al.*, 2010a] for determination of the pore space filled by hydrate. The DAPC consists of a core cutting barrel and a pressure chamber for gas-tight sealing of the sediment core at in situ hydrostatic pressure. While the DAPC is in its working principle similar to a conventional piston corer, the degree of sediment overpenetration is insignificant. The nominal capacity of the core liner is ca. 12 L. Gas volumes contained in individual pressure cores were specified by incremental degassing using the method described by *Pape et al.* [2010b]. The analytical precision of this technique is estimated at <3 vol% of the total gas volume released from the pressure core [*Pape et al.*, 2011]. Water volumes pushed through the manifold during degassing are equivalent to gas volumes released and were, thus, added to yield the total gas volume.

[16] For onshore analysis of the molecular composition of the sedimentary gas, gas subsamples were taken at selected pressure levels prevailing inside the pressure chamber with a gas-tight syringe and transferred into sealed glass vials as described above. The molecular composition of light hydrocarbons was determined by gas chromatography [*Pape et al.*, 2010a; *Pape et al.*, 2010b] within six weeks after sampling. Average proportions (*Gc*) of individual hydrocarbons and carbon dioxide for the series of gas subsamples released from pressurized sediment cores were calculated according to

$$Gc = \sum_{i=1}^{n} (GC_i * (G_{vi} - G_{vi-1})) / \sum_{i=1}^{n} (G_{vi} - G_{vi-1}) \quad (1)$$

where GC_i is the portion of the specific compound (%) in each subsample (i) and G_{vi} is the accumulated gas volume released when the subsample was taken [*Heeschen et al.*, 2007; *Pape et al.*, 2010a].

[17] Total gas volumes in pressure cores (V_{tg}) were assigned to volumes of free gas and cumulative gas volumes comprising hydrate-bound and dissolved gas with regard to pressure-volume relationships recorded during core degassing according to *Dickens et al.* [2000], *Dickens et al.* [2003], *Milkov et al.* [2004a], and *Pape et al.* [2010b]. In addition, methane concentrations exceeding solubilities in the presence of a hydrate phase (48.1 mmol L^{-1} pore volume) [*Tishchenko et al.*, 2005] were assumed to be liberated entirely from hydrates.

[18] Subsequently, the gas volumes were converted into methane volumes considering the molecular gas composition (Table 3). Because we did not analyze for all volatiles typically contained in MV associated fluids (e.g., hydrocarbons, CO_2, H_2S),

Table 4. In Situ Sediment Temperature Measurements Used to Compile a Map of Near-Seabed Geothermal Gradient at the Håkon Mosby Mud Volcano

Year	Cruise	Vessel	GCT[a]	T-Stick[a]	HF Probe[a]
2003	ARK-XIX/3b	R/V *Polarstern*	2[b]	33[b]	66 (3 m)[c]
2005	AWIROV	R/V *L'Atalante*	–	16[b]	–
2006	VICKING	R/V *Pourquoi Pas?*	5[b]	24[b]	–
2007	ARK-XXII/1b	R/V *Polarstern*	4[d]	24[e]	–
2009	ARK-XXIV/2	R/V *Polarstern*		–	33 (6 m)[d]

[a]"GCT" denotes gravity corers equipped with autonomous temperature loggers mounted on outriggers, "T-Stick" refers to various types of short temperature probes operated by remotely operated vehicles (ROVs), and "HF Probe" stands for two standard violin bow type heat flow probes of 3 and 6 m length [*Feseker et al.*, 2008]. A complete list of all in situ sediment temperature measurements used to compile the map of the temperature gradient at the seabed is provided in the auxiliary material.
[b]*Feseker et al.* [2008].
[c]*Kaul et al.* [2006].
[d]Previously unpublished data collected by T. Feseker.
[e]*Perez-Garcia et al.* [2009].

methane is assumed to constitute 95% of the volume of all gas compounds. Stable carbon isotope ratios of methane were determined as reported elsewhere [*Pape et al.*, 2010a].

[19] Volumes of hydrate-bound and dissolved methane were referred to core segments potentially comprising hydrates, i.e., those in between the temperature-related BGHSZ and the base of the SZ. Although absolute sulfate depletion was observed for none of our pressure cores, we defined the base of the SZ in sediments to be positioned below the steepest concentration gradients. Hydrate fractions (in % pore volume) in the respective core segments were calculated using an estimated sediment porosity φ of 0.7 and converting methane concentrations exceeding equilibrium [*Tishchenko et al.*, 2005] into gas hydrate volumes using a hydration number of 6.1, which is typical for natural sI hydrates [*Ripmeester and Ratcliffe*, 1988]. For core segments lacking gas hydrates, i.e., within the SZ, methane solubilities were calculated according to *Duan and Mao* [2006]. Gas hydrate phase boundaries in HMMV near-surface sediments were calculated using the HWHYD U.K. software [*Masoudi and Tohidi*, 2005; *Østergaard et al.*, 2005] loaded with molecular compositions of hydrate-bound volatiles (Table 3) and salinities of interstitial waters.

[20] After termination of the pressure core degassing procedure, the core liner was removed from the DAPC pressure chamber and opened. Pore water was taken at selected depth intervals using the Rhizon technique [*Seeberg-Elverfeldt et al.*, 2005] and transferred into sample vials. Chloride and sulfate concentrations in pore water were measured by ion chromatography using a METROHM 761 Compact IC equipped with a 788 IC Filtration Sample Processor autosampler.

2.2.2. In Situ Sediment Temperature Measurements

[21] In situ sediment temperature measurements at the HMMV were obtained during five cruises between 2003 and 2007 (Table 4). In this study we combine in situ temperature measurements from the literature [*Feseker et al.*, 2008; *Kaul et al.*, 2006; *Perez-Garcia et al.*, 2009] with as yet unpublished data. These in situ sediment temperature measurements were obtained during cruise ARK-XXII/1b in 2007 using 6 autonomous temperature loggers mounted on outriggers that were welded on the barrel of a 5.75 m long GC lowered into the sediment with the ship's wire. Measuring at a resolution of 0.0006°C and a precision of 0.002°C, the loggers were programmed to record temperature readings with 0.2 Hz during the entire deployment. For each measurement, the GC was left in the sediment for a period of 10 min in order for the sensors to adjust to ambient temperature. A pressure sensor and a tiltmeter were used to document the entire deployment.

[22] Additional measurements with a violin bow type heat flow probe were obtained during cruise ARK-XXIV/2 in 2009. The instrument was equipped with 22 temperature sensors distributed over an active length of 5.46 m. Measuring at a resolution of 0.0006°C, the sensors were calibrated to a precision of 0.003°C. Additional sensors for acceleration, tilt, and bottom water temperature were used to control the measurements. At each station, the heat flow probe remained in the sediment for around 7 min in order for the sensors to adjust to ambient sediment temperature. During all measurements, the data was transmitted from the probe to the winch control room in real time via the ship's cable. For all deployments of the GC and the heat flow probe, equilibrium sediment tem-

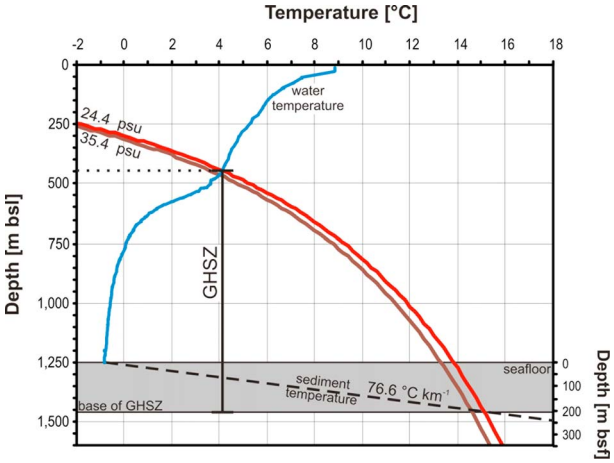

Figure 4. Phase boundaries of the nominal gas hydrate stability zone calculated for gas hydrate structure I at the HMMV using bottom water (35.4 psu) and fluid salinity (24.4 psu as revealed from cores DAPC 2 and 5), temperature (–0.83°C), pressure and gas chemical data obtained during ARK-XXII/1b in summer 2007. For overview, the dashed line indicates a hypothetical geothermal gradient of 0.076°C m^{-1} which is considered as background value.

peratures were calculated by extrapolation from the recorded time series [*Villinger and Davis*, 1987].

2.2.3. Gas Hydrate Stability in Shallow Sediments of the HMMV

[23] The three-dimensional extent of the GHOZ at the HMMV was calculated from the temperature gradient at the seafloor, the microbathymetry, and the mean bottom water temperature. A map of geothermal gradients at the seabed was compiled from selected in situ sediment temperature measurements. Data obtained from short temperature probes operated by a remotely operated vehicle (ROV) provided precise information about the geothermal gradient directly at the seabed. In contrast, measurements collected using other instruments such as GCs equipped with autonomous temperature loggers and standard heat flow probes were often affected by overpenetration and showed nonlinear temperature profiles. Therefore, many available temperature profiles particularly from the MV center had to be excluded. Out of 91 in situ sediment temperature measurements published by *Kaul et al.* [2006], 25 measurements were discarded in the context of this study because a temperature of more than 0°C at the topmost sensor indicated that the heat flow probe assembly had overpenetrated. Based on all stations at which the geothermal gradient at the seabed could be derived, a map was interpolated for the entire MV on a 5 m grid by kriging with automated parameter estimation using the package "intamap" (E. Pebesma et al., intamap: Procedures for automated interpolation, R package version 1.3–4, 2010, available at http://CRAN.R-project.org/package=intamap) in R [*R Development Core Team*, 2010]. This map of the temperature gradient at the seabed was subsequently combined with microbathymetry data compiled in 2003 [*Foucher et al.*, 2009] and the mean bottom water temperature of –0.83°C in order to calculate the depth of the BGHSZ for pure methane hydrates and sulfate-free pore water at a salinity of 35 PSU following the Pitzer approach [*Tishchenko et al.*, 2005].

3. Results and Discussion

3.1. Composition of Light Hydrocarbons and Hydrate Crystallographic Structure

[24] Average hydrocarbon compositions in gas subsamples taken during degassing of pressure cores from Units I and II were strongly dominated by methane (>99.919 mol % of C_1 to *n*-C_4 alkanes (Table 3). This was followed by ethane (C_2, 0.078 mol %) and propane (C_3, 0.002 mol %). Molecular hydrocarbon compositions (C_1/C_{2+} = 1,018 to 1,542) and δ^{13}C-CH_4 values (approx. –63.9‰ V-PDB) suggest that methane obtained from the pressure cores primarily originated from microbial processes such as carbonate reduction.

[25] Hydrate-bound gas was generally more enriched in methane than gases released from pressurized cores (Table 3), which also include non-hydrate-bound hydrocarbons, indicating preferential methane incorporation into the hydrate phase. The relative methane enrichment in shallow hydrates is likely due to molecular fractionation during hydrate precipitation and microbial consumption of dissolved methane present in pressure cores [*Pape et al.*, 2010a]. Hydrocarbon compositions along with pore water salinity in depressurized cores, and bottom water temperatures plotted in Figure 4 suggest structure I (sI) hydrates to be the most stable hydrate structure at the HMMV. Preponderance of sI hydrates at the HMMV has already been reported by *Chazallon et al.* [2007] using micro-Raman spectroscopy. In the HMMV area, the dissociation temperature of sI hydrates is approx. 13.8°C, which is 14.6°C higher than the bottom water temperature (Figure 4). These hydrates should generally be stable in waters below approx.

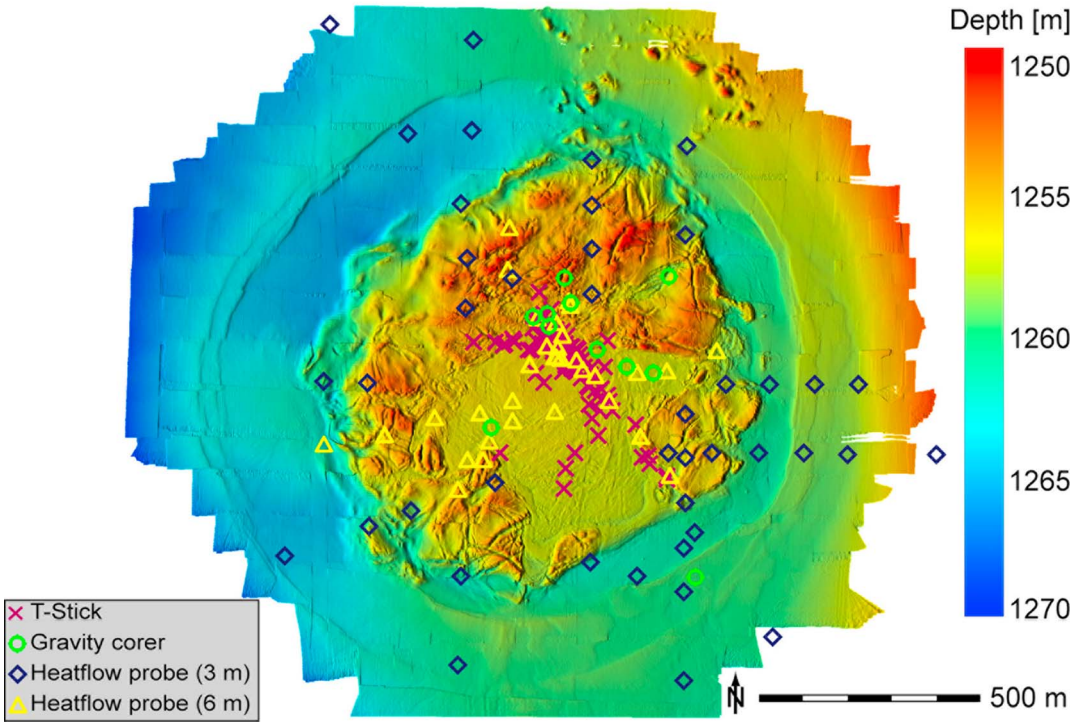

Figure 5. Locations of in situ sediment temperature measurements using short temperature lances ('T-Stick'; red crosses) operated with an ROV, heat flow probes of different length (blue diamonds and yellow triangles) and gravity corers equipped with autonomous temperature loggers (green circles) (microbathymetry data from *Foucher et al.* [2009]).

450 m bsl, at typical temperature-salinity conditions. In 2007, shallow hydrates (>40 cm bsf) were found in seven GCs taken in deposits belonging to Units I and II (Figure 3 and Table 1).

3.2. Spatial Boundaries of Gas Hydrate Occurrences

3.2.1. Map of the Geothermal Gradient at the Seabed

[26] During cruise ARK-XXII/1b, 15 in situ sediment temperature measurements were conducted using the 5.75 m GC. Measurements from GCs which showed overpenetration were not used, because they did not provide reliable information on the temperature gradient at the sediment-water interface. At four stations in Unit II north of the geometric center with proper penetration temperature gradients ranged between 1 and 2.6°C m^{-1}.

[27] Real-time data transmission from the heat flow probe to the ship allowed for a much better control of the measurements during cruise ARK-XXIV/2 and resulted in 33 successful stations. Geothermal gradients at the sediment-water interface ranged between 0.1°C m^{-1} at the MV edges and 40°C m^{-1} close to the MV center. The positions and inter-

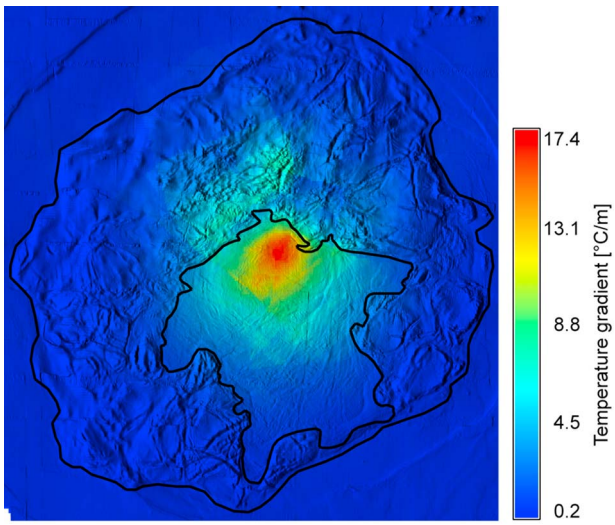

Figure 6. Maps of interpolated geothermal gradient at the seabed on a 5 m grid.

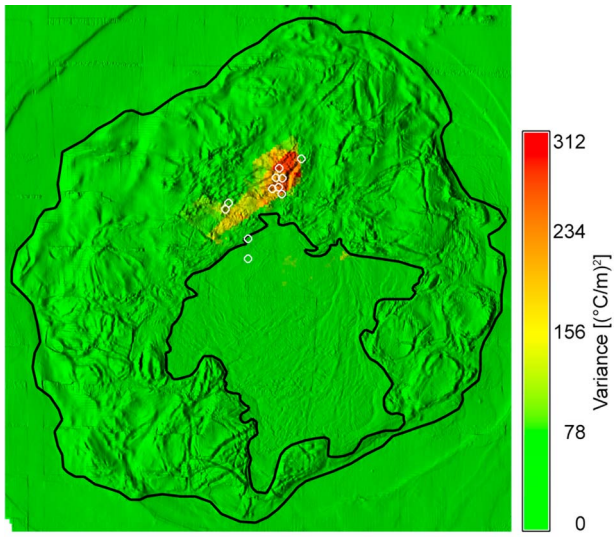

Figure 7. Map of the kriging variance of the interpolated geothermal gradient used in Figure 6. The white circles indicate locations where gas ebullition was observed during ROV-based seafloor inspections in 2003 [*Foucher et al.*, 2010; *Sauter et al.*, 2006]. Shaded relief based on microbathymetry data from *Foucher et al.* [2009].

preted temperature gradients for all successful stations are listed along with the temperature gradients for previously published data which are provided in the auxiliary material.[1]

[28] An overview of all 207 in situ temperature measurements used in this study is given in Figure 5. The geothermal gradient at the seabed ranges from 46°C m^{-1} at the center to 0.0420°C m^{-1} at a distance of 3.5 km from the MV center. While the highest values were always measured near the geometric center (Unit I), the temperature gradient is subject to very high variability in both space and time, as the MV was more or less active in terms of fluid and/or gas expulsion during the different cruises [cf. *Feseker et al.*, 2008]. Therefore, the map compiled from this data depicts an average distribution of temperature gradients observed between 2003 and 2007. As shown in Figure 6, the highest average temperature gradients of up to 17.4°C m^{-1} were found around the geometric center. This indicates that the most active area of the HMMV is located almost in the geographic center in the northern part of the flat area (Unit I). To the north, the boundary between Units I and II is associated with an abrupt decrease in temperature gradient, while the southward decrease in temperature gradient away from the center within Unit I is much more gradual. The map suggests the presence of a secondary warm area north-northwest of the geometric center, which is also associated with the highest kriging variance (Figure 7). As this area coincides with the locations where *Sauter et al.* [2006] and *Foucher et al.* [2010] observed massive gas bubble release in 2003 and 2006, respectively, the high variance is thought to reflect temporal variability rather than poor data quality. Further away from the center, the temperature gradient decreases to values of around 0.18°C m^{-1}.

3.2.2. Thickness of the Gas Hydrate Occurrence Zone

[29] Phase calculations indicate that gas hydrates are stable in sediments close to the seafloor across the entire MV at temperatures below 13.8°C (Figure 4). Considering hydrostatic pressure, and assuming constant and homogeneous bottom water temperature, and sulfate-free pore water at a salinity of 35 PSU, the Pitzer approach [*Tishchenko et al.*, 2005] was applied to estimate the thickness of the GHOZ from the microbathymetry and the geothermal gradient in the seabed on a 5 m grid. Due to poor data coverage for the outer parts of the HMMV, the estimation is confined to the morphological Units I and II. As illustrated in Figure 8, the thickness of the GHOZ ranges between 0.8 and 27 m

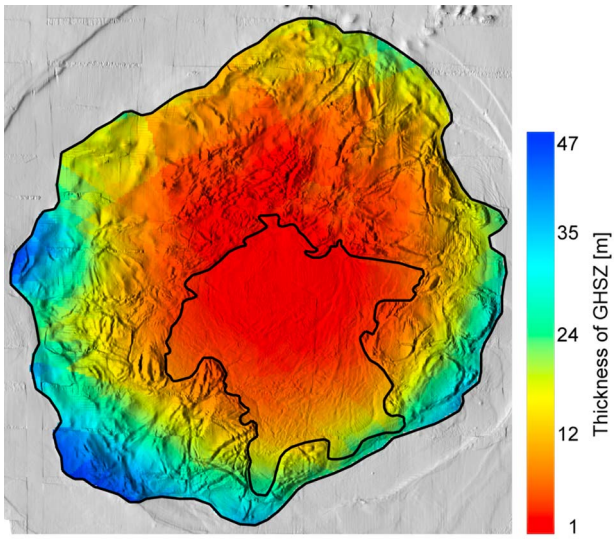

Figure 8. Thickness of the GHOZ in the morphological Units I and II (shaded relief based on microbathymetry data from *Foucher et al.* [2009]).

[1]Auxiliary materials are available in the HTML. doi:10.1029/2011GC003575.

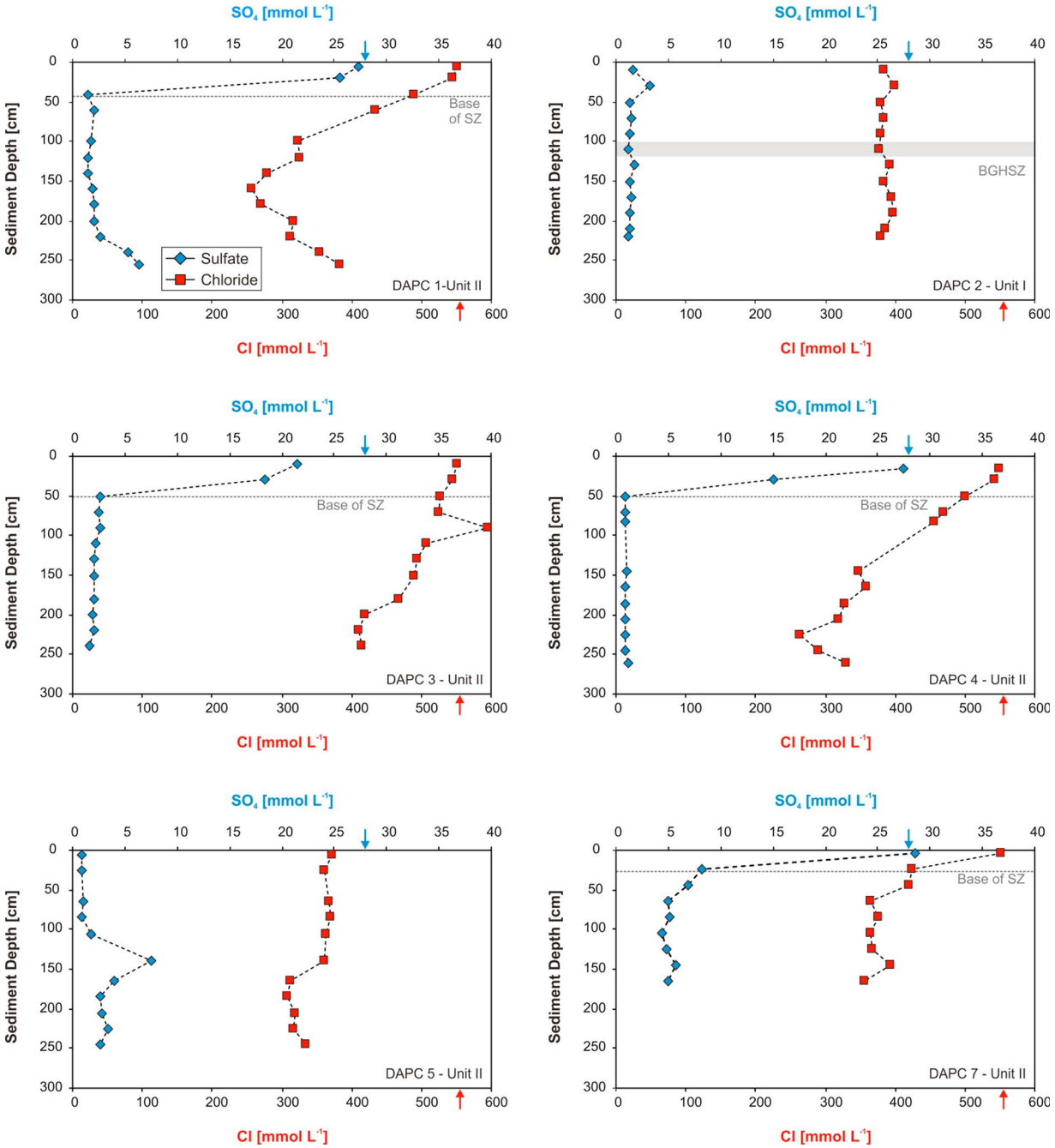

Figure 9. Depth profiles of chloride and sulfate determined for pressurized sediment cores upon depressurization. Blue and red arrows indicate bottom water sulfate and chloride concentrations, respectively. Dashed lines and grey horizontal bar in profiles indicate the base of the sulfate zone (SZ) and base of the GHSZ, respectively. For core DAPC 6, pore water profiles were not analyzed, since only a voluminous sediment-water suspension was left in the core liner after depressurization.

in Unit I and between 1.2 and 47 m in Unit II. Thus, despite the high temperature gradients in the central area the map predicts that hydrates are stable within a thin layer below the sediment surface, which is corroborated by the recovery of cm-sized hydrate aggregates in GCs (GC 3, 4, and 5) taken at the geometric center (Table 1).

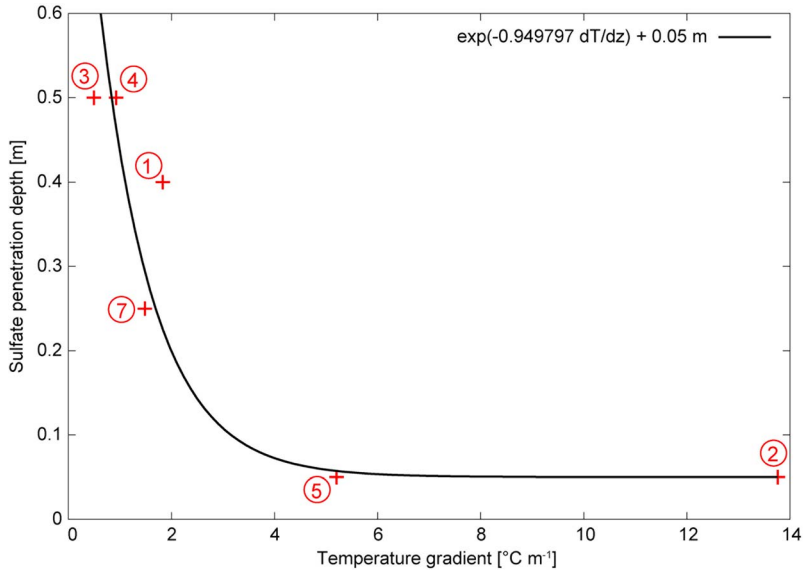

Figure 10. An exponential transfer function was fitted to the ratios of sulfate penetration and geothermal gradient as revealed for individual sites at the seabed (red crosses; DAPC core numbers indicated in circles) in order to map the base of the sulfate zone (SZ) as the top of the GHOZ at the HMMV.

3.2.3. Sulfate Penetration and the Upper Boundary of the Gas Hydrate Occurrence Zone

[30] As expected, during ARK-XXII/1b a downward diffusive sulfate penetration was not observed in the geometric center (core DAPC 2 (Unit I; Figures 3 and 9) and core DAPC 5 (Unit II close to Unit I)). However, sulfate penetration reached down to about 20 cm bsf in core DAPC 7 (Unit II) taken in the southwestern section of the HMMV structure. In cores taken in the northern section, such as DAPC 1, 3, and 4 (Unit II), sulfate reached down to about 50 cm bsf substantiating deepening of the SZ toward the outer regions of the MV structure. These observations are consistent with pore water sulfate concentration profiles determined during several previous cruises and might be explained by diminished fluid flux from below at the periphery in combination with bioirrigation caused by siboglinid tubeworms [*de Beer et al.*, 2006; *Felden et al.*, 2010; *Lichtschlag et al.*, 2010; *Niemann et al.*, 2006b].

[31] For assessing the thickness of the GHOZ, in this study the top of the GHOZ was defined as the base of the SZ. It should be noted that this approach might result in a slight overestimation of the thickness of the GHOZ and in conservative calculations of hydrate fractions in the pore space. This is because typically a cm to dm thick interval exists between the base of the SZ and the top of the GHOZ which is characterized by the absence of sulfate and hydrates (see Figure 1) and the presence of methane exclusively in the dissolved phase. For mapping the base of the SZ, the sulfate penetration depth from individual pressure cores was correlated with site-specific geothermal gradients. Assuming that the upward fluid flux controls both the temperature distribution in shallow sediments and the diffusive downward flux of sulfate [*Borowski et al.*, 1996], sulfate penetration for unsampled locations was estimated from the geothermal gradient in the seabed. Figure 10 shows that the sulfate penetration depth measured in each DAPC core and the corresponding site-specific estimate of the geothermal gradient may be described by the following transfer function:

$$z\_SO_4 = \exp\left(-0.949797\,\mathrm{m^2/K} * \mathrm{dT/dz}\right) + 0.05\,\mathrm{m} \quad (2)$$

where z_SO_4 is the sulfate penetration depth [in m] and dT/dz is the estimate of the geothermal gradient [in °C m^{-1}] at the seabed. Note that even though sulfate penetration was not observed in the cores taken from the central area, the transfer function implies a minimum penetration depth of 0.05 m (Figure 10). Using equation (2), z_SO_4 was estimated for Units I and II from the geothermal gradient at the seabed on a 5 m grid. Estimates range from the minimum sulfate penetration of 0.05 m at the center to a maximum penetration of 0.66 and 0.8 m in Units I and II, respectively. Bathymetry,

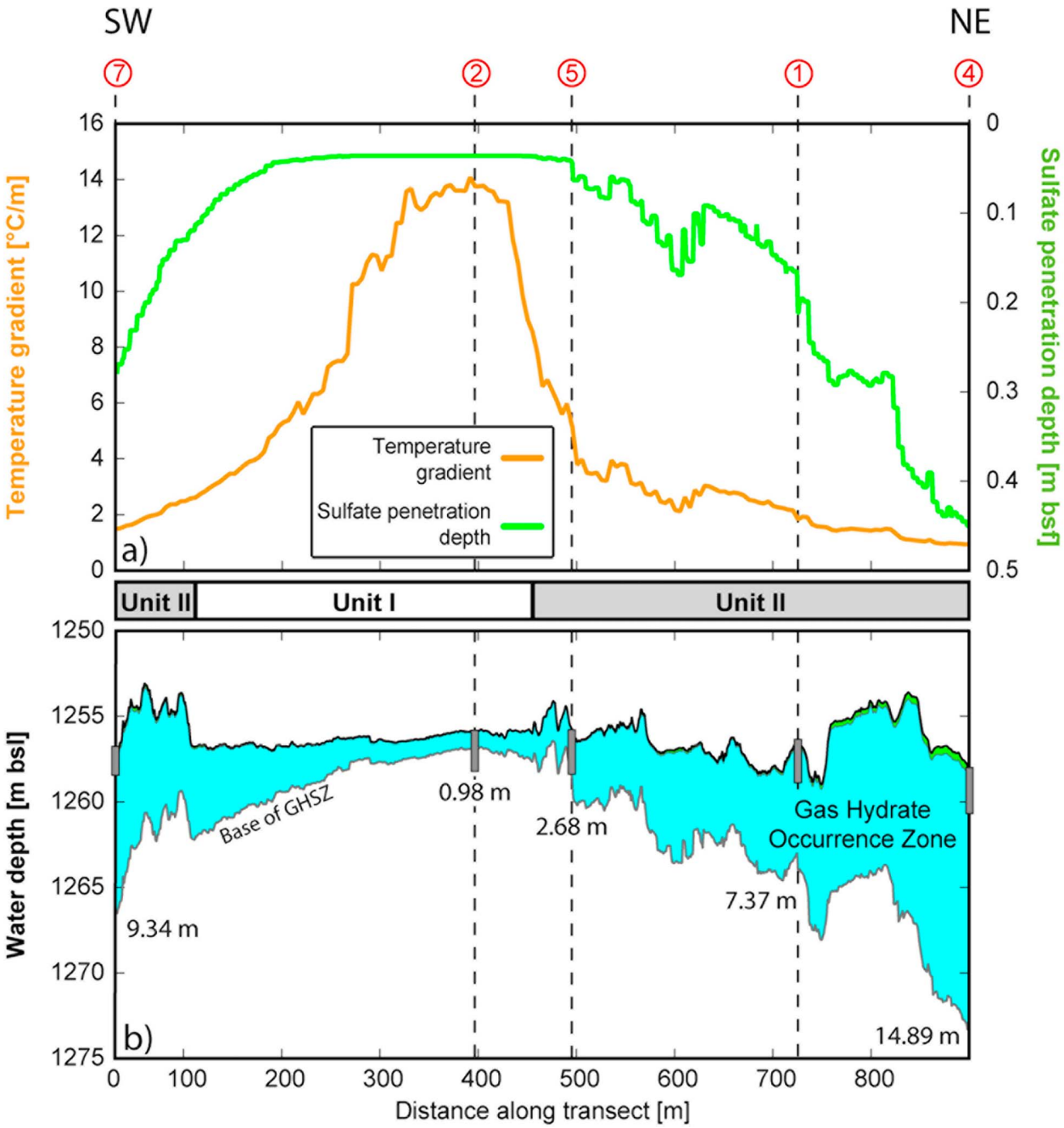

Figure 11. (a) Sulfate penetration depth (green line) and temperature gradient (brown line) as well as (b) thickness of the sulfate zone (green shading) and the GHOZ (blue shading) along the SW-NE trending profile line (based on micro-bathymetry data from *Foucher et al.* [2009]) through the locations of pressure coring and covering morphological Units I and II. The black line represents the sediment surface and the gray line the BGHSZ. Pressure cores are depicted as gray bars; bar length corresponds to corer penetration depth. Values indicate the thickness of the GHOZ in meters at the respective pressure core stations.

geothermal gradients, and sulfate penetration along with the resulting GHOZ are illustrated along a transect line connecting the locations of five DAPC cores in Figure 3. The vertical hydrate distributions in shallow deposits of the HMMV are highlighted by the profile in Figure 11, which closely resembles the assumed watch glass–like distribution of hydrates as depicted in Figure 1.

Table 5. Gas and Gas Hydrate Contents in Pressurized Cores Taken From the HMMV During ARK-XXII/1b[a]

	DAPC						Mean
	2	1	3	4	5	7	(n = 5)
Morphological unit	I	II	II	II	II	II	
Core length below SZ (cm)	235	215	215	220	255	125	
Bulk sediment volume below SZ (mL)	12,556	11,487	11,487	11,754	13,624	6,679	
Pore volume below SZ (mL)	8,789	8,041	8,041	8,228	9,537	5,423	
Proportion free gas (vol %)	7.3	0.5	4.4	0.8	4.6	3.4	
Amount hydrate-bound CH_4 (mol)	2.25	9.30	1.05	7.95	7.85	9.15	
Mass hydrate-bound CH_4 (g)	36.1	149.3	16.81	127.5	125.9	146.7	
Concentration hydrate-bound methane per pore volume (mol L^{-1})	0.256	1.157	0.130	0.966	0.823	1.686	
Volume gas hydrate (mL)	284.8	1176.4	132.5	1004.8	992.5	1156.4	
Hydrate fraction in bulk sediment below SZ (vol %)	2.3	10.2	1.2	8.5	7.3	14.9	8.7
Hydrate fraction in pore volume below SZ (vol %)	3.2	14.6	1.6	12.2	10.4	21.3	12.5

[a]SZ, sulfate zone. Proportion free gas in vol % of total gas volume (V_{tg}). The extent of analytical uncertainties is discussed in section 3.4.2.

3.3. In Situ Gas and Gas Hydrate Densities in Individual Pressure Cores

3.3.1. Gas Volumes and Methane Concentrations

[32] Five out of the seven DAPC stations achieved nearly full core recovery (ca. 2.65 m, Table 2) indicating that corer penetration was not significantly impeded by resistant material, such as massive accumulations of authigenic carbonates or gas hydrates. Total gas volumes V_{tg} released from the pressurized sediment cores ranged between 37.2 L for core DAPC 3 taken at the northwestern outer rim, and 231.2 L for core DAPC 1 recovered in the northeastern section of the HMMV (Table 2).

[33] Comparison of core lengths and local GHOZ thicknesses (Figure 11) suggests that only DAPC 2 taken in the HMMV center penetrated the BGHSZ. The volumetric gas–sediment ratio below the SZ ranged between 2.6 (DAPC 3) and 25.2 (DAPC 7; Table 2), with the latter value clearly indicating the presence of hydrates. For core DAPC 6 (ca. 190 L of gas), which was taken close to the warm area in Unit II northwest of the center including gas bubble sites (Figures 3 and 7), the sediment volume could only be estimated. After degassing, a fluid sediment-water suspension was left in the core liner, most probably due to the presence of hydrates in high density. Thus, a volumetric gas–sediment ratio of 70.7 assumed for this station is a rough estimate, and data from this core were not considered for hydrate-related calculations.

[34] Considering lower and upper boundaries of the GHOZ (section 3.2), V_{tg} and methane concentrations were related to the respective core segments. Consequently, concentrations of hydrate-bound methane ranged between 130 mmol L^{-1} pore volume (pv) for DAPC 3 and 1,686 mmol L^{-1} pv in DAPC 7, both cores taken from Unit II deposits (Table 5). Concentrations of hydrate-bound methane for DAPC 2 recovered from the center (Unit I) were 256 mmol L^{-1} pv. Core DAPC 5, taken close to the Unit I/II boundary, revealed concentrations of hydrate-bound methane of 823 mmol L^{-1} pv.

[35] So far, gas hydrate inventories calculated from DAPC cores were reported for two seep sites in the Northern Gulf of Mexico [*Heeschen et al.*, 2007], the Amsterdam MV in the Eastern Mediterranean [*Pape et al.*, 2010b], the Batumi cold seep area [*Pape et al.*, 2011], and the Dvurechenskii MV [*Feseker et al.*, 2009b] with the latter two located in the Black Sea. Compared to the reported values, DAPC 1 investigated in this study contained highest overall concentrations of hydrate-bound methane (9.3 M; Table 5). In addition, methane concentrations calculated for near-surface pressure cores are in the same order of magnitude as maximum methane concentrations reported for deep sediments at other submarine hydrocarbon seeps like the Blake Ridge (2.0 M) [*Dickens et al.*, 1997], Peru Trench (0.4 M) [*Dickens et al.*, 2003], Hydrate Ridge (3.1 M) [*Milkov et al.*, 2003a], and Northern Cascadia Margin (3.8 M) [*Riedel et al.*, 2006].

3.3.2. Gas Hydrate Contents Calculated From Methane Concentrations

[36] Hydrate fractions calculated for hydrate-bearing segments in the six pressure cores considered (except for DAPC 6) were on average 12.5% pv (Table 5).

The highest hydrate fraction of 21.3% pv was measured for DAPC 7 (Unit II), while the lowest hydrate abundance was determined for DAPC 3 (1.6% pv) taken from the outer edge of Unit II. The only core recovered from Unit I, DAPC 2, yielded a hydrate fraction of 3.2% pv. The average hydrate fractions observed in this study for hydrate-bearing near-seafloor segments are similar to those determined by pressure coring at other hydrate-bearing sites, like the Batumi seep area [*Pape et al.*, 2011], the Hydrate Ridge (mean ~11%pv) [*Milkov et al.*, 2003a], the Northern Gulf of Mexico (max. 18% pv) [*Heeschen et al.*, 2007], or the Blake Ridge (max. 9%pv) [*Dickens et al.*, 1997].

3.4. Estimates of Overall Methane Amounts in Shallow Gas Hydrates at the HMMV

3.4.1. Quantification of Hydrate-Bound Methane

[37] The total volume of the GHOZ within Units I and II amounts to approx. 1.1 * 10^7 m^3, of which ca. 1.8 * 10^6 m^3 are located less than 2.65 mbsf and, thus, within reach of the DAPC (Table 6). Total unit-specific hydrate and methane volumes were calculated according to *Pape et al.* [2011] considering estimated sediment porosity (φ = 0.7) and in situ hydrate densities as revealed from the pressure coring (section 3.3.1). Considering the maximum DAPC penetration depth (265 cm), such calculations resulted in 8,892 m^3 of hydrates (1.5 * 10^6 m^3 of hydrate-bound methane at STP, respectively) for Unit I and hydrate volumes of 118,791 m^3 (1.9 * 10^7 m^3 of hydrate-bound methane at STP) for Unit II (Table 6). These volumes sum up to 127,684 m^3 of hydrates (15.0 kt of hydrate-bound methane) for the upper 2.65 m in HMMV deposits belonging to the morphological Units I and II. Such amounts of methane bound in shallow deposits assigned to Unit I and II at the HMMV (ca. 0.81 km^2; Table 6) in 2007 are similar to those established for the Batumi seep area (ca. 0.5 km^2; 11.3 kt of hydrate-bound methane [*Pape et al.*, 2011]). When calculating hydrate amounts expanding to the BGHSZ the total hydrate volume would sum up to 8.7 * 10^5 m^3 (102.5 kt of hydrate-bound methane). With respect to the molecular composition of hydrate-bound hydrocarbons determined in this study (Table 3), about 130 t of ethane are additionally fixed in the sI hydrates (Table 6).

[38] The total amount of hydrate-bound methane in Unit I and Unit II sediments (6.4 * 10^9 mol; this study) is 340- and 470-fold larger, respectively than estimates of methane annually released in the gaseous phase (1.9 * 10^7 mol yr^{-1}) [*Sauter et al.*, 2006] and diffusive methane effluxes (1.4 * 10^7 mol yr^{-1}) [*Felden et al.*, 2010]. For liberating significant amounts of hydrate-bound methane (3.2 * 10^7 mol) equaling those considered to be annually released in the gaseous and diffusive phase, dissociation of approximately half of the hydrates stored in Unit I of the HMMV is needed. These calculations indicate that hydrates in Units I and II of the HMMV have a great storage capacity for volatile hydrocarbons, which in particular in the dynamic central part of the MV [cf. *Foucher et al.*, 2010] might be instantaneously subject to decomposition during a typical eruptive phase, when sediment temperature surpasses hydrate dissociation temperatures.

3.4.2. Analysis of Uncertainty

[39] The estimates of the amount and spatial distribution of gas hydrates at the HMMV presented above are based on a large number of different parameters, and each of these parameters is associated with uncertainty. The depth of the BGHSZ was derived from the bathymetry and an interpolated map of the geothermal gradient at the seabed. While the microbathymetry data from *Foucher et al.* [2009] used in this study presents an accurate map of the HMMV in summer 2003, the method applied here could not account for changes in the morphology of the MV due to eruptive activity. The map of the thermal gradients in the seabed is based on all in situ temperature measurements that were available hitherto. Even though each of these individual measurements provides a highly accurate value of the geothermal gradient, the interpolation is associated with a large uncertainty: The precision of positioning ranged from around 30 m to less than 10 m, depending on whether the ship's GPS position or the ultra short baseline navigation system was used. However, it is known from in situ sediment temperature measurements conducted during ROV dives that particularly in the central area, the spatial variability in the geothermal gradient exceeds the precision of positioning in either case. In addition, the temperature measurements used in this study were collected during different cruises to the HMMV between 2003 and 2009 and thus reflect different phases of mud volcanic activity [*Feseker et al.*, 2008]. As a result, the map of the geothermal gradient represents an interpolation from accurate geothermal gradients at uncertain positions, integrated over a period of 6 years, and it is clear that the true temperature distribution at any single point

Table 6. Gas Hydrate–Related Details of Unit I and Unit II Deposits at the Håkon Mosby Mud Volcano

Parameter	Unit I	Unit II	Σ Unit I+II
Area (m^2)	176,385	632,745	809,130
Temperature gradient (K m^{-1})			
Min	0.512	0.307	
Max	17.442	11.812	
Mean	4.574	1.537	2.200
SO_4 penetration depth (m)			
Min	0.05	0.05	
Max	0.61	0.79	
Mean	0.16	0.40	0.35
Base of GHSZ (mbsf)			
Min	0.81	1.20	
Max	28.09	47.32	
Mean	6.02	15.74	13.61
Thickness of GHOZ (m)			
Min	0.76	1.15	
Max	27.44	46.54	
Mean	5.86	15.34	13.26
Volume of GHOZ (m^3)			
Min	134,053	727,657	
Max	4,840,004	29,447,952	
Mean	1,033,616	9,706,308	10,729,064
Volume of GHOZ above 2.65 mbsf (m^3)	391,961	1,360,352	1,751,101
Porosity	0.7	0.7	0.7
Pore volume within GHOZ (m^3)			
Min	93,837	509,360	
Max	3,388,003	20,613,567	
Mean	723,531	6,794,416	7,510,345
Pore volume within GHOZ above 2.65 mbsf (m^3)	274,373	952,246	1,226,619
Hydrate fraction within GHOZ above 2.65 mbsf (% of pv) (see Table 5)			
Min		1.6	
Max		21.3	
Mean	3.2	12.5	
Volume gas hydrate within GHOZ[b,c] (m^3)	23,449	847,594	871,043
Volume gas hydrate within GHOZ above 2.65 mbsf[c] (m^3)	8,892	118,791	127,684
Mass gas hydrates within GHOZ[b,c] (kt)	21.4	774.7	7796.1
Mass gas hydrates within GHOZ above 2.65 mbsf[c] (kt)	8.1	108.6	116.7
Volume hydrate-bound CH_4 within GHOZ[b,c,d] (m^3)	3,845,677	139,005,376	142,841,053
Volume hydrate-bound CH_4 within GHOZ above 2.65 mbsf[c,d] (m^3)	1,458332	19,481,788	20,940,120
Mass hydrate-bound CH_4 within GHOZ[b,c] (kt)	2.8	99.7	102.5
Mass hydrate-bound CH_4 within GHOZ above 2.65 mbsf[c] (kt)	1.0	14.0	15.0
Amount hydrate-bound CH_4 within GHOZ[b,c] (mol)	171,989,110	6,216,698,399	6,388,687,510
Amount hydrate-bound CH_4 within GHOZ above 2.65 mbsf[c] (mol)	65,220,563	871,278,538	936,499,100
Mass hydrate-bound C_2H_6 within GHOZ[b,c] (t)	3.4	126.3	129.8
Mass hydrate-bound C_2H_6 within GHOZ above 2.65 mbsf[c] (t)	1.3	17.7	19.0

[a]The extent of analytical uncertainties is discussed in section 3.4.2; pv, pore volume.
[b]Assuming identical hydrate fractions in shallow and in deeper sediments.
[c]Considering mean values.
[d]At standard temperature and pressure (STP).

in time will deviate significantly from this approximation. In the central area, e.g., measurements indicated peak gradients of more than 40°C/m [*Feseker et al.*, 2008], while the interpolated map shows a maximum temperature gradient of less than 20°C/m. Close to the edges of the mud volcano, scarcity of measurements probably caused overestimation of the geothermal gradient. Nonetheless, we are confident that this map describes the mean temperature distribution for the period of time from which the observations were taken.

[40] The upper limit of the GHOZ was defined as the base of the sulfate zone (SZ). Due to a lack of

sufficient pore water data for most areas of the mud volcano, sulfate penetration was calculated from the geothermal gradient (Figure 10). Based on pore water profiles from 6 gravity corer stations and interpolated geothermal gradients for the positions of these stations, the transfer function was applied to the area of the entire mud volcano, which is obviously associated with large uncertainty.

[41] The exact depth of the base of the SZ is difficult to identify in the pressure cores (Figure 9) due to two aspects: On the one hand sulfate concentrations in all cores are in the millimolar range even below the assumed SZ, i.e., an unambiguous zone where sulfate is consumed to depletion is absent in all cores. On the other hand the sampling resolution applied in this study does not allow to accurately identify the depth of the reaction zone where sulfate is reduced with methane. Assuming that AOM is the main sulfate consuming process, the interval with the steepest sulfate gradient indicates the base of the SZ [e.g., *Bhatnagar et al.*, 2011]. We therefore decided to use the steepest gradients of the sulfate profiles in Figure 9 as indicators for the base of the SZ in the respective cores.

[42] In addition, the analytical error arising from calculation of gas hydrate amounts from overall gas volumes obtained during pressure core degassing (i.e., reading error, determinations of relative proportions of free gas, hydrate-bound gas and dissolved gas from degassing characteristics, assignment of hydrate crystallographic structure) is estimated to amount to 5 vol% of the total gas hydrate volume.

[43] In summary, the overall uncertainty cannot be quantified, but we are confident that our estimates should be within 25% of the true mean hydrate concentration at the HMMV.

3.4.3. Relationship Between Hydrate Occurrence and Pore Water Chloride Profiles

[44] The volume of hydrate-bound methane calculated to be present in Unit I and II ($1.4 * 10^8$ m^3) on the base of our direct measurements is in the same order of magnitude as that previously calculated for the entire HMMV structure (i.e., including Unit III) on the base of pore water chloride profiles ($3 * 10^8$ m^3) [*Ginsburg et al.*, 1999]. Nevertheless, estimates of hydrate concentrations based on pore water chlorinity are problematic as the shape of such profiles and the magnitude of the chloride anomalies are strongly affected by the age of the hydrate system [e.g., *Hiruta et al.*, 2009]. While negative ex situ anomalies in chloride concentrations are expected for relatively mature hydrate deposits due to ion exclusion during hydrate precipitation and loss by advection and/or diffusion [*Hesse*, 2003; *Ussler and Paull*, 2001], ex situ pore water chloride concentrations might only be slightly diminished in relatively young hydrate systems. For instance, in this study total gas volumes (V_{tg}) obtained during pressure core degassing (section 3.3.1) and modeling of the GHOZ (sections 3.2.2 and 3.2.3) clearly indicate the presence of hydrates in near-surface deposits within or close to the HMMV center (cores DAPC 2, Unit I; and DAPC 5, Unit II), although chloride concentration profiles of these cores do not show hydrate-related pore water freshening (Figure 9). In contrast, conspicuous ex situ negative chloride anomalies revealing in situ hydrate occurrences were found for all cores taken beyond the center (DAPC 1, 4 and 7).

[45] These observations demonstrate that for accurate calculations of hydrate pore volume saturations based on pore water chloride anomalies hydrate ages must be considered. Similar conclusions were drawn from correlations between gas volume-based hydrate densities and pore water profiles determined for the Amsterdam MV located in the Eastern Mediterranean [*Pape et al.*, 2010b]. Nevertheless, most previous studies concerned with estimates of hydrate-bound methane at MV structures are based on pore water calculations [*Ginsburg et al.*, 1999; *Mazurenko et al.*, 2003]. Consequently, the uncertainty of estimates of global amounts of MV associated hydrates could be higher than previously thought.

[46] The absence of negative pore water chloride anomalies in the depressurized cores (DAPC 2 and 5) shows that despite relatively high rates of pore water flux, in situ positive pore water chloride anomalies resulting from hydrate formation have not been attenuated by diffusion or advection. This suggests that precipitation of hydrates at the HMMV center started in (sub)recent times and that since their formation there was not enough time available to level off the positive in situ chloride anomaly by molecular diffusion. This interpretation is corroborated by previously published indications of relatively recent mud volcanic eruptions [*Foucher et al.*, 2010; *Kaul et al.*, 2006].

4. Conclusions

[47] Under the pressure regime present at the Håkon Mosby Mud Volcano (HMMV), gas hydrates of the

crystallographic structure I are stable up to about 13.8°C. The thickness of the hydrate stability zone is controlled by the temperature distribution in the sediment and ranges between less than 1 m at the center belonging to the morphological Unit I and more than 45 m at the outer limit of Unit II. The upper limit of the gas hydrate occurrence zone is determined by the sulfate penetration depth, which in turn depends on seepage rates and is thus related to the geothermal gradient. In contrast to earlier studies, which assumed the general absence of hydrates in the warm center of the HMMV, we show that hydrates can exist in a thin layer near the sediment surface despite extremely high geothermal gradients. Our data suggests that sulfate penetration increases exponentially with decreasing temperature gradient. Consequently, both the depth and the thickness of the GHOZ increase away from the center.

[48] Well-defined methane and gas hydrate inventories for the near-surface sediments of the HMMV are provided. Hydrate volumes below the sulfate zone ranged between 1.6 and 21.3% of pore volume with highest densities found for a station in the morphological Unit II southwest of the geometrical center. The total volume of hydrate-bound methane ($1.4 * 10^8$ m^3 at standard temperature and pressure) precisely determined by our investigations is in the order of the estimate ($3 * 10^8$ m^3 STP) reported in a previous study on the base of pore water chemistry exclusively. Nonetheless, the present study, which combined in situ methane concentrations, molecular hydrocarbon compositions, sediment temperature gradients, and concentrations of pore water constituents, demonstrates that detailed knowledge of the spatial distribution of shallow hydrates is crucial for assessing their thermodynamic stability and their potential to release significant amounts of methane during mud volcanic eruptions.

[49] During phases of mud volcanic activity enhanced seepage will lead to increasing temperatures in shallow sediments and thus induce the decomposition of shallow hydrates at and close to the central area of the HMMV, resulting in the liberation of methane into overlying sediments and the bottom water. Decomposition of only half of the hydrates stored in Unit I of the HMMV is required to release amounts of hydrate-bound methane equaling those estimated to be annually released in the gaseous and diffusive phase ($3.2 * 10^7$ mol) from the entire mud volcano structure in previous studies.

[50] The absence of chloride anomalies in the depressurized cores retrieved from the central area of the mud volcano indicates that the in situ pore water composition is not in equilibrium and suggests a relatively young age of the sampled hydrates. Episodic mud volcanic activity is likely to cause frequent cycles of dissociation and formation of hydrates particularly in the central area of the MV, resulting in a highly dynamic gas hydrate system.

Acknowledgments

[51] We acknowledge the captains and crews of the R/V *Polarstern* (cruises ARK-XIX/3b, ARK-XXII/1b), R/V *L'Atalante* (AWI-ROV), and R/V *Pourquoi Pas?* (VICKING) for excellent collaboration during field work. The skill and experience of the crews of the ROV *Victor 6000* (IFREMER, Brest) and ROV *QUEST 4000m* (MARUM, Bremen) made it possible to obtain such a large number of measurements during the dives. We thank M. Klages (chief scientist; Alfred Wegener Institute for Polar and Marine Research, Bremerhaven) and F. Wenzhöfer (co–chief scientist; Max Planck Institute for Marine Microbiology, Bremen) for supporting DAPC deployments during cruise ARK-XXII/1b. H.-J. Hohnberg and F. Abegg (MARUM) are greatly acknowledged for preparation and deployments of the DAPC. N. Vetz is thanked for gas molecular analysis. We are very thankful to I. R. MacDonald (Florida State University) and T. D. Lorenson (USGS Coastal and Marine Surveys) for constructive comments and language support that considerably improved the quality of the manuscript. This work was prepared through financial support from the European Commission's Framework Six Program 'Hot spot Ecosystems Research on the Margins of European Seas' HERMES (GOCE-CT-2005-511234-1). The study was also funded through the Helmholtz Association (Alfred Wegener Institute for Polar and Marine Research, Bremerhaven). This is contribution GEOTECH-1531 of the R&D program GEOTECHNOLOGIEN funded by the German Ministry of Education and Research (BMBF) and the German Research Foundation (DFG), collaborative project METRO (grant 03G0604A), and through DFG-Research Center/Cluster of Excellence "MARUM–The Ocean in the Earth System."

References

Abegg, F., H. J. Hohnberg, T. Pape, G. Bohrmann, and J. Freitag (2008), Development and application of pressure-core-sampling systems for the investigation of gas- and gas-hydrate-bearing sediments, *Deep Sea Res., Part I*, *55*(11), 1590–1599, doi:10.1016/j.dsr.2008.06.006.

Barnes, R. O., and E. D. Goldberg (1976), Methane production and consumption in anaerobic marine sediments, *Geology*, *4*(5), 297–300, doi:10.1130/0091-7613(1976)4<297:MPACIA>2.0.CO;2.

Bhatnagar, G., S. Chatterjee, W. G. Chapman, B. Dugan, G. R. Dickens, and G. J. Hirasaki (2011), Analytical theory relating the depth of the sulfate-methane transition to gas hydrate distribution and saturation, *Geochem. Geophys. Geosyst.*, *12*, Q03003, doi:10.1029/2010GC003397.

Blinova, V., M. Ivanov, and G. Bohrmann (2003), Hydrocarbon gases in deposits from mud volcanoes in the Sorokin Trough, north-eastern Black Sea, *Geo Mar. Lett.*, *23*(3–4), 250–257, doi:10.1007/s00367-003-0148-8.

Bohrmann, G., and M. E. Torres (2006), Gas hydrates in marine sediments, in Marine Geochemistry, edited by H. D. Schulz and M. Zabel, pp. 481–512, Springer, Heidelberg, Germany, doi:10.1007/3-540-32144-6_14.

Bohrmann, G., et al. (2003), Mud volcanoes and gas hydrates in the Black Sea: New data from Dvurechenskii and Odessa mud volcanoes, *Geo Mar. Lett.*, *23*(3–4), 239–249, doi:10.1007/s00367-003-0157-7.

Borowski, W. S., C. K. Paull, and W. Ussler III (1996), Marine pore-water sulfate profiles indicate in situ methane flux from underlying gas hydrate, *Geology*, *24*(7), 655–658, doi:10.1130/0091-7613(1996)024<0655:MPWSPI>2.3.CO;2.

Charlou, J. L., J. P. Donval, T. Zitter, N. Roy, P. Jean-Baptiste, J. P. Foucher, and J. Woodside (2003), Evidence of methane venting and geochemistry of brines on mud volcanoes of the eastern Mediterranean Sea, *Deep Sea Res., Part I*, *50*(8), 941–958, doi:10.1016/S0967-0637(03)00093-1.

Charlou, J. L., J. P. Donval, C. Bourry, C. Chaduteau, N. Lanteri, L. Bignon, J. P. Foucher, H. Nouzé, and Vicking Scientific Team (2007), Gas bubbles and gas hydrates sampling from Hakon Mosby Mud Volcano–Preliminary results–VICKING cruise (2006), *Geophys. Res. Abstr.*, *9*, 08690.

Chazallon, B., C. Focsa, J.-L. Charlou, C. Bourry, and J.-P. Donval (2007), A comparative Raman spectroscopic study of natural gas hydrates collected at different geological sites, *Chem. Geol.*, *244*(1–2), 175–185, doi:10.1016/j.chemgeo.2007.06.012.

Damm, E., and G. Budeus (2003), Fate of vent-derived methane in seawater above the Hakon Mosby mud volcano (Norwegian Sea), *Mar. Chem.*, *82*(1–2), 1–11, doi:10.1016/S0304-4203(03)00031-8.

de Beer, D., E. Sauter, H. Niemann, N. Kaul, J.-P. Foucher, U. Witte, M. Schlüter, and A. Boetius (2006), In situ fluxes and zonation of microbial activity in surface sediments of the Håkon Mosby Mud Volcano, *Limnol. Oceanogr.*, *51*(3), 1315–1331, doi:10.4319/lo.2006.51.3.1315.

Deville, E., and S. H. Guerlais (2009), Cyclic activity of mud volcanoes: Evidences from Trinidad (SE Caribbean), *Mar. Pet. Geol.*, *26*(9), 1681–1691, doi:10.1016/j.marpetgeo.2009.03.002.

Dickens, G. R., C. R. Paull, P. Wallace, and the ODP Leg 164 Scientific Party (1997), Direct measurement of *in situ* methane quantities in a large gas-hydrate reservoir, *Nature*, *385*(6615), 426–428, doi:10.1038/385426a0.

Dickens, G. R., P. J. Wallace, C. K. Paull, and W. S. Borowski (2000), Detection of methane gas hydrate in the pressure core sampler (PCS): Volume-pressure-time relations during controlled degassing experiments, *Proc. Ocean Drill. Program Sci. Results*, *164*, 113–126.

Dickens, G. R., D. Schroeder, K.-U. Hinrichs, and the Leg 201 Scientific Party (2003), The pressure core sampler (PCS) on ODP Leg 201: General operations and gas release, *Proc. Ocean Drill. Program Initial Rep.*, *201*, 1–22.

Dimitrov, L. I. (2002), Mud volcanoes—The most important pathway for degassing deeply buried sediments, *Earth Sci. Rev.*, *59*(1–4), 49–76, doi:10.1016/S0012-8252(02)00069-7.

Dimitrov, L. I. (2003), Mud volcanoes—A significant source of atmospheric methane, *Geo Mar. Lett.*, *23*, 155–161, doi:10.1007/s00367-003-0140-3.

Duan, Z., and S. Mao (2006), A thermodynamic model for calculating methane solubility, density and gas phase composition of methane-bearing aqueous fluids from 273 to 523 K and from 1 to 2000 bar, *Geochim. Cosmochim. Acta*, *70*(13), 3369–3386, doi:10.1016/j.gca.2006.03.018.

Egorov, A. V., K. Crane, P. R. Vogt, A. N. Rozhkov, and P. P. Shirshov (1999), Gas hydrates that outcrop on the sea floor: Stability models, *Geo Mar. Lett.*, *19*(1–2), 68–75.

Elvert, M., and H. Niemann (2008), Occurrence of unusual steroids and hopanoids derived from aerobic methanotrophs at an active marine mud volcano, *Org. Geochem.*, *39*(2), 167–177, doi:10.1016/j.orggeochem.2007.11.006.

Etiope, G., and P. Ciccioli (2009), Earth's degassing: A missing ethane and propane source, *Science*, *323*(5913), 478, doi:10.1126/science.1165904.

Etiope, G., and R. W. Klusman (2002), Geologic emissions of methane to the atmosphere, *Chemosphere*, *49*, 777–789, doi:10.1016/S0045-6535(02)00380-6.

Etiope, G., K. R. Lassey, R. W. Klusman, and E. Boschi (2008), Reappraisal of the fossil methane budget and related emission from geologic sources, *Geophys. Res. Lett.*, *35*, L09307, doi:10.1029/2008GL033623.

Felden, J., F. Wenzhöfer, T. Feseker, and A. Boetius (2010), Transport and consumption of oxygen and methane in different habitats of the Håkon Mosby Mud Volcano, *Limnol. Oceanogr.*, *55*(6), 2366–2380, doi:10.4319/lo.2010.55.6.2366.

Feseker, T., J. P. Foucher, and F. Harmegnies (2008), Fluid flow or mud eruptions? Sediment temperature distributions on Håkon Mosby mud volcano, SW Barents Sea slope, *Mar. Geol.*, *247*(3–4), 194–207, doi:10.1016/j.margeo.2007.09.005.

Feseker, T., A. Dählmann, J. P. Foucher, and F. Harmegnies (2009a), In-situ sediment temperature measurements and geochemical porewater data suggest highly dynamic fluid flow at Isis mud volcano, eastern Mediterranean Sea, *Mar. Geol.*, *261*(1–4), 128–137, doi:10.1016/j.margeo.2008.09.003.

Feseker, T., T. Pape, K. Wallmann, S. A. Klapp, F. Schmidt-Schierhorn, and G. Bohrmann (2009b), The thermal structure of the Dvurechenskii mud volcano and its implications for gas hydrate stability and eruption dynamics, *Mar. Pet. Geol.*, *26*(9), 1812–1823, doi:10.1016/j.marpetgeo. 2009.01.021.

Foucher, J. P., G.-H. Westbrook, A. Boetius, S. Ceramicola, S. Dupré, J. Mascel, J. Mienert, O. Pfannkuche, C. Pierre, and D. Praeg (2009), Structure and drivers of cold seep ecosystems, *Oceanography*, *22*(1), 84–101.

Foucher, J.-P., S. Dupré, C. Scalabrin, T. Feseker, F. Harmegnies, and H. Nouzé (2010), Changes in seabed morphology, mud temperature and free gas venting at the Håkon Mosby mud volcano, offshore northern Norway, over the time period 2003–2006, *Geo Mar. Lett.*, *30*(3–4), 157–167, doi:10.1007/s00367-010-0193-z.

Ginsburg, G. D., A. V. Milkov, V. A. Soloviev, A. V. Egorov, G. A. Cherkashev, P. R. Vogt, K. Crane, T. D. Lorenson, and M. D. Khutorskoy (1999), Gas hydrate accumulation at the Håkon Mosby Mud Volcano, *Geo Mar. Lett.*, *19*(1–2), 57–67.

Greinert, J., Y. Artemov, V. Egorov, M. De Batist, and D. McGinnis (2006), 1300-m-high rising bubbles from mud volcanoes at 2080 m in the Black Sea: Hydroacoustic characteristics and temporal variability, *Earth Planet. Sci. Lett.*, *244*(1–2), 1–15, doi:10.1016/j.epsl.2006.02.011.

Hanson, R. S., and T. E. Hanson (1996), Methanotrophic bacteria, *Microbiol. Rev.*, *60*(2), 439–471.

Heeschen, K. U., H. J. Hohnberg, M. Haeckel, F. Abegg, M. Drews, and G. Bohrmann (2007), In situ hydrocarbon concentrations from pressurized cores in surface sediments,

northern Gulf of Mexico, *Mar. Chem.*, *107*(4), 498–515, doi:10.1016/j.marchem.2007.08.008.

Hesse, R. (2003), Pore water anomalies of submarine gas-hydrate zones as tool to assess hydrate abundance and distribution in the subsurface: What have we learned in the past decade?, *Earth Sci. Rev.*, *61*(1–2), 149–179, doi:10.1016/S0012-8252(02)00117-4.

Hiruta, A., G. T. Snyder, H. Tomaru, and R. Matsumoto (2009), Geochemical constraints for the formation and dissociation of gas hydrate in an area of high methane flux, eastern margin of the Japan Sea, *Earth Planet. Sci. Lett.*, *279*(3–4), 326–339, doi:10.1016/j.epsl.2009.01.015.

Hjelstuen, B. O., O. Eldholm, J. I. Faleide, and P. R. Vogt (1999), Regional setting of Hakon Mosby Mud Volcano, SW Barents Sea margin, *Geo Mar. Lett.*, *19*(1–2), 22–28.

Hoehler, T. M., M. J. Alperin, D. B. Albert, and C. S. Martens (1994), Field and laboratory studies of methane oxidation in an anoxic marine sediment: Evidence for a methanogen-sulfate reducer consortium, *Global Biogeochem. Cycles*, *8*(4), 451–463, doi:10.1029/94GB01800.

Ivanov, M. K., A. F. Limonov, and T. C. E. van Weering (1996), Comparative characteristics of the Black Sea and Mediterranean Ridge mud volcanoes, *Mar. Geol.*, *132*, 253–271, doi:10.1016/0025-3227(96)00165-X.

Jerosch, K., M. Schlüter, J.-P. Foucher, A.-G. Allais, M. Klages, and C. Edy (2007), Spatial distribution of mud flows, chemoautotrophic communities, and biogeochemical habitats at Håkon Mosby Mud Volcano, *Mar. Geol.*, *243*(1–4), 1–17, doi:10.1016/j.margeo.2007.03.010.

Kaul, N., J. P. Foucher, and M. Heesemann (2006), Estimating mud expulsion rates from temperature measurements on Håkon Mosby Mud Volcano, SW Barents Sea, *Mar. Geol.*, *229*(1–2), 1–14, doi:10.1016/j.margeo.2006.02.004.

Kopf, A. J. (2002), Significance of mud volcanism, *Rev. Geophys.*, *40*(2), 1005, doi:10.1029/2000RG000093.

Kopf, A. J. (2003), Global methane emission through mud volcanoes and its past and present impact on the Earth's climate, *Int. J. Earth Sci.*, *92*(5), 806–816.

Kvenvolden, K. A. (1988), Methane hydrate—A major reservoir of carbon in the shallow geosphere?, *Chem. Geol.*, *71*, 41–51, doi:10.1016/0009-2541(88)90104-0.

Kvenvolden, K. A., and B. W. Rogers (2005), Gaia's breath—Global methane exhalations, *Mar. Pet. Geol.*, *22*(4), 579–590, doi:10.1016/j.marpetgeo.2004.08.004.

Lein, A., P. Vogt, K. Crane, A. Egorov, and M. Ivanov (1999), Chemical and isotopic evidence for the nature of the fluid in CH_4-containing sediments of the Hakon Mosby Mud Volcano, *Geo Mar. Lett.*, *19*(1–2), 76–83.

Lichtschlag, A., J. Felden, V. Brüchert, A. Boetius, and D. de Beer (2010), Geochemical process and chemosynthetic primary production in different thiotrophic mats of the Håkon Mosby Mud Volcano (Barents Sea), *Limnol. Oceanogr.*, *55*(2), 931–949, doi:10.4319/lo.2009.55.2.0931.

Limonov, A. F., J. M. Woodside, and M. K. Ivanov (1994), Mud volcanism in the Mediterranean and Black seas and shallow structure of the Eratosthenes Seamount. Initial results of the geological and geophysical investigations during the third UNESCO-ESF 'Training-through-Research' cruise of RV Gelendzhik (June-July 1993), *Rep. Mar. Sci.*, *64*, 173 pp., U.N. Educ., Sci., and Cult. Organ., Paris.

Lösekann, T., K. Knittel, T. Nadalig, B. Fuchs, H. Niemann, A. Boetius, and R. Amann (2007), Diversity and abundance of aerobic and anaerobic methane oxidizers at the Haakon Mosby Mud Volcano, Barents Sea, *Appl. Environ. Microbiol.*, *73*(10), 3348–3362, doi:10.1128/AEM.00016-07.

Masoudi, R., and B. Tohidi (2005), Estimating the hydrate stability zone in the presence of salts and/or organic inhibitors using water partial pressure, *J. Pet. Sci. Eng.*, *46*(1–2), 23–36, doi:10.1016/j.petrol.2004.10.002.

Mastalerz, V., G. J. de Lange, A. Dählmann, and T. Feseker (2007), Active venting at the Isis mud volcano, offshore Egypt: Origin and migration of hydrocarbons, *Chem. Geol.*, *246*(1–2), 87–106, doi:10.1016/j.chemgeo.2007.09.005.

Mazurenko, L. L., V. A. Soloviev, J. M. Gardner, and M. K. Ivanov (2003), Gas hydrates in the Ginsburg and Yuma mud volcano sediments (Moroccan Margin): Results of chemical and isotopic studies of pore water, *Mar. Geol.*, *195*(1–4), 201–210, doi:10.1016/S0025-3227(02)00688-6.

Milkov, A. V. (2000), Worldwide distribution of submarine mud volcanoes and associated gas hydrates, *Mar. Geol.*, *167*(1–2), 29–42, doi:10.1016/S0025-3227(00)00022-0.

Milkov, A. V. (2004), Global estimates of hydrate-bound gas in marine sediments: How much is really out there?, *Earth Sci. Rev.*, *66*, 183–197, doi:10.1016/j.earscirev.2003.11.002.

Milkov, A. V., and G. Etiope (2005), Global methane emission through mud volcanoes and its past and present impact on the Earth's climate—A comment, *Int. J. Earth Sci.*, *94*(3), 490–492.

Milkov, A. V., P. Vogt, G. Cherkashev, G. Ginsburg, N. Chernova, and A. Andriashev (1999), Sea-floor terrains of Hakon Mosby Mud Volcano as surveyed by deep-tow video and still photography, *Geo Mar. Lett.*, *19*(1–2), 38–47.

Milkov, A. V., G. E. Claypool, Y.-J. Lee, W. Xu, G. R. Dickens, W. S. Borowski, and the ODP Leg 204 Scientific Party (2003a), In situ methane concentrations at Hydrate Ridge, offshore Oregon: New constraints on the global gas hydrate inventory from an active margin, *Geology*, *31*(10), 833–836, doi:10.1130/G19689.1.

Milkov, A. V., R. Sassen, T. V. Apanasovich, and F. G. Dadashev (2003b), Global gas flux from mud volcanoes: A significant source of fossil methane in the atmosphere and the ocean, *Geophys. Res. Lett.*, *30*(2), 1037, doi:10.1029/2002GL016358.

Milkov, A. V., G. R. Dickens, G. E. Claypool, Y.-J. Lee, W. S. Borowski, M. E. Torres, W. Xu, H. Tomaru, A. M. Tréhu, and P. Schultheiss (2004a), Co-existence of gas hydrate, free gas, and brine within the regional gas hydrate stability zone at Hydrate Ridge (Oregon margin): Evidence from prolonged degassing of a pressurized core, *Earth Planet. Sci. Lett.*, *222*(3–4), 829–843, doi:10.1016/j.epsl.2004.03.028.

Milkov, A. V., P. R. Vogt, K. Crane, A. Y. Lein, R. Sassen, and G. A. Cherkashev (2004b), Geological, geochemical, and microbial processes at the hydrate-bearing Hakon Mosby mud volcano: A review, *Chem. Geol.*, *205*(3–4), 347–366, doi:10.1016/j.chemgeo.2003.12.030.

Niemann, H., J. Duarte, C. Hensen, E. Omoregie, V. H. Magalhaes, M. Elvert, L. M. Pinheiro, A. Kopf, and A. Boetius (2006a), Microbial methane turnover at mud volcanoes of the Gulf of Cadiz, *Geochim. Cosmochim. Acta*, *70*(21), 5336–5355, doi:10.1016/j.gca.2006.08.010.

Niemann, H., et al. (2006b), Novel microbial communities of the Haakon Mosby mud volcano and their role as a methane sink, *Nature*, *443*(7113), 854–858, doi:10.1038/nature05227.

Østergaard, K. K., R. Masoudi, B. Tohidi, A. Danesh, and A. C. Todd (2005), A general correlation for predicting the suppression of hydrate dissociation temperature in the presence of thermodynamic inhibitors, *J. Pet. Sci. Eng.*, *48*(1–2), 70–80, doi:10.1016/j.petrol.2005.04.002.

Pape, T., A. Bahr, J. Rethemeyer, J. D. Kessler, H. Sahling, K. U. Hinrichs, S. A. Klapp, W. S. Reeburgh, and G. Bohrmann (2010a), Molecular and isotopic partitioning of low-molecular weight hydrocarbons during migration and gas hydrate precip-

itation in deposits of a high-flux seepage site, *Chem. Geol.*, *269*(3–4), 350–363, doi:10.1016/j.chemgeo.2009.10.009.

Pape, T., S. Kasten, M. Zabel, A. Bahr, F. Abegg, H.-J. Hohnberg, and G. Bohrmann (2010b), Gas hydrates in shallow deposits of the Amsterdam mud volcano, Anaximander Mountains, northeastern Mediterranean Sea, *Geo Mar. Lett.*, *30*(3–4), 187–206, doi:10.1007/s00367-010-0197-8.

Pape, T., A. Bahr, S. A. Klapp, F. Abegg, and G. Bohrmann (2011), High-intensity gas seepage causes rafting of shallow gas hydrates in the southeastern Black Sea, *Earth Planet. Sci. Lett.*, *307*, 35–46, doi:10.1016/j.epsl.2011.04.030.

Paull, C., W. Ussler III, T. Lorenson, W. Winters, and J. Dougherty (2005), Geochemical constraints on the distribution of gas hydrates in the Gulf of Mexico, *Geo Mar. Lett.*, *25*(5), 273–280, doi:10.1007/s00367-005-0001-3.

Perez-Garcia, C., T. Feseker, J. Mienert, and C. Berndt (2009), The Håkon Mosby mud volcano: 330 000 years of focused fluid flow activity at the SW Barents Sea slope, *Mar. Geol.*, *262*(1–4), 105–115, doi:10.1016/j.margeo.2009.03.022.

R Development Core Team (2010), *R: A Language and Environment for Statistical Computing*, R Found. for Stat. Comput., Vienna. [Available at http://www.R-project.org]

Reeburgh, W. S. (1976), Methane consumption in Cariaco Trench waters and sediments, *Earth Planet. Sci. Lett.*, *28*(3), 337–344, doi:10.1016/0012-821X(76)90195-3.

Riedel, M., T. S. Collett, M. J. Malone, and Expedition 311 Scientists (2006), *Proceedings of the Integrated Ocean Drilling Program*, vol. 311, Integrated Ocean Drill. Program, College Station, Tex.

Ripmeester, J. A., and C. I. Ratcliffe (1988), Low-temperature cross-polarization/magic angle spinning ^{13}C NMR of solid methane hydrates: Structure, cage occupancy, and hydration number, *J. Phys. Chem.*, *92*, 337–339, doi:10.1021/j100313a018.

Sahling, H., et al. (2009), Vodyanitskii Mud Volcano, Sorokin Trough, Black Sea: Geological characterization and quantification of gas bubble streams, *Mar. Pet. Geol.*, *26*(9), 1799–1811, doi:10.1016/j.marpetgeo.2009.01.010.

Sauter, E. J., S. I. Muyakshin, J.-L. Charlou, M. Schlüter, A. Boetius, K. Jerosch, E. Damm, J.-P. Foucher, and M. Klages (2006), Methane discharge from a deep-sea submarine mud volcano into the upper water column by gas hydrate-coated methane bubbles, *Earth Planet. Sci. Lett.*, *243*(3–4), 354–365, doi:10.1016/j.epsl.2006.01.041.

Seeberg-Elverfeldt, J., M. Schlüter, T. Feseker, and M. Kölling (2005), Rhizon sampling of porewaters near the sediment-water interface of aquatic systems, *Limnol. Oceanogr. Methods*, *3*, 361–371, doi:10.4319/lom.2005.3.361.

Sloan, E. D., and C. A. Koh (2007), *Clathrate Hydrates of Natural Gases*, 3rd ed., 752 pp., CRC Press, Boca Raton, Fla.

Stadnitskaia, A., M. K. Ivanov, V. Blinova, R. Kreulen, and T. C. E. van Weering (2006), Molecular and carbon isotopic variability of hydrocarbon gases from mud volcanoes in the Gulf of Cadiz, NE Atlantic, *Mar. Pet. Geol.*, *23*(3), 281–296, doi:10.1016/j.marpetgeo.2005.11.001.

Tishchenko, P., C. Hensen, K. Wallmann, and C. S. Wong (2005), Calculation of the stability and solubility of methane hydrate in seawater, *Chem. Geol.*, *219*, 37–52, doi:10.1016/j.chemgeo.2005.02.008.

Ussler, W., III, and C. K. Paull (2001), Ion exclusion associated with marine gas hydrate deposits, in *Natural Gas Hydrates: Occurrence, Distribution and Detection*, *Geophys. Monogr. Ser.*, vol. 124, edited by C. K. Paull and W. P. Dillon, pp. 41–52, AGU, Washington, D. C.

Vanneste, H., B. A. Kelly Gerreyn, D. P. Connelly, R. H. James, M. Haeckel, R. E. Fisher, K. Heeschen, and R. A. Mills (2011), Spatial variation in fluid flow and geochemical fluxes across the sediment-seawater interface at the Carlos Ribeiro mud volcano (Gulf of Cadiz), *Geochim. Cosmochim. Acta*, *75*(4), 1124–1144, doi:10.1016/j.gca.2010.11.017.

Villinger, H., and E. E. Davis (1987), A new reduction algorithm for marine heat flow measurements, *J. Geophys. Res.*, *92*(B12), 12,846–12,856, doi:10.1029/JB092iB12p12846.

Vogt, P. R., G. Cherkashev, G. Ginsburg, G. Ivanov, A. Milkov, K. Crane, A. Lein, E. Sundvor, N. Pimenov, and A. Egorov (1997), Haakon Mosby Mud Volcano provides unusual example of venting, *Eos Trans. AGU*, *78*(48), 549.

Woodside, J. M., M. K. Ivanov, A. F. Limonov, and Shipboard Scientists of the Anaxiprobe Expeditions (1998), Shallow gas and gas hydrates in the Anaximander Mountains region, eastern Mediterranean Sea, in *Gas Hydrates: Relevance to World Margin Stability and Climate Change*, edited by J.-P. Henriet and J. Mienert, pp. 177–193, Geol. Soc., London.